DEVELOPMENT OF A DOUBLE-OBLIQUE-SHOCK SCRAMJET MODEL IN A SHOCK TUNNEL

I. T. Osgerby, H. K. Smithson and D. A. Wagner
ARO, Inc.

August 1969

VON KÁRMÁN GAS DYNAMICS FACILITY
ARNOLD ENGINEERING DEVELOPMENT CENTER
AIR FORCE SYSTEMS COMMAND
ARNOLD AIR FORCE STATION, TENNESSEE

DEVELOPMENT OF A DOUBLE-OBLIQUE-SHOCK SCRAMJET MODEL IN A SHOCK TUNNEL

I. T. Osgerby, H. K. Smithson and D. A. Wagner
ARO, Inc.

FOREWORD

The research reported herein was sponsored by the Arnold Engineering Development Center (AEDC), Air Force Systems Command (AFSC), under Program Element 62402F, Project 3012, Task 07.

The results of research reported herein were obtained by ARO, Inc. (a subsidiary of Sverdrup & Parcel and Associates, Inc.), contract operator of AEDC, AFSC, Arnold Air Force Station, Tennessee, under Contract F40600-69-C-0001. The work was performed under ARO Project Nos. VT5822 and VT5922 from February 1967 to September 1968. The manuscript was submitted for publication on February 13, 1969.

The authors wish to thank the many people who participated in this research work and in particular the contributions of J. T. Rose, the tunnel engineer, and A. H. Boudreau who collected the original ramp pressure and heat-transfer data.

This technical report has been reviewed and is approved.

Forrest B. Smith, Jr.
Research Division
Directorate of Plans
and Technology

Harry L. Maynard
Colonel, USAF
Director of Plans
and Technology

ABSTRACT

A double-oblique-shock scramjet model has been developed using the AEDC-VKF 16-in. Shock Tunnel I at a free-stream Mach number of 11. The model was developed as a test bed for the development of instrumentation and hydrogen fuel injection techniques for supersonic combustion experiments to be conducted at the 54-in. test section in the AEDC-VKF Tunnel F. Difficulties were encountered, especially at the entrance to the combustor because of the combined action of separation and the interaction of the second shock from the cowl lip. Considerable effort was expended before these influences were reduced to the point that the flow in the combustor was satifactory. The results of these development tests are reported here.

CONTENTS

APPENDIXES

I. ILLUSTRATIONS

Figure

NOMENCLATURE

1s through 5s	Shock tube notation, see Fig. 2
A	Area
C_H	Stanton number
C_f	Skin friction coefficient
ER	Equivalence ratio
H	Total specific enthalpy
h	Specific enthalpy
M	Mach number
Pr	Prandtl number
p	Pressure
$\dot{q}_w$	Heat-transfer rate per unit area to wall
R	Universal gas constant
Re	Reynolds number
S	Entropy
T	Temperature
U	Flow velocity
X	Distance from plate leading edge or combustor entrance
γ	Ratio of specific heats
δ	Flow deflection angle
δ^*	Boundary-layer displacement thickness
μ	Viscosity or Prandtl-Meyer expansion angle
ρ	Density
τ_{id}	Ignition delay time
τ_R	Reaction time

SUBSCRIPTS

o	Reservoir (total) condition
∞	Free-stream condition in tunnel test section

2 (or R)	Conditions on the ramp inlet behind the first oblique shock
3 (or C)	Conditions in the combustor behind the second oblique shock
ex	Conditions at the exit plane of the combustor
ℓ	Laminar boundary layer
r	Recovery value
t	Turbulent boundary layer
w	Wall condition
x	Denotes a local value

SUPERSCRIPTS

$'$	Value behind a normal shock
*	Conditions at M = 1, or property evaluated at the Eckert reference enthalpy

SECTION I
INTRODUCTION

The principal conclusion of many authors of papers pertaining to supersonic combustion ramjet (scramjet) engines is that there is a tremendous potential in such a propulsion device for efficient, economic (relative to rockets) transportation of payload if very high engine component efficiencies can be realized. This is particularly so for the hypersonic inlet which must be capable of producing two to three orders of magnitude change in static pressure level with significantly less than an order of magnitude change in total pressure level, and all to be accomplished at hypersonic Mach numbers! This kind of performance efficiency will only be achieved by extensive experimental testing of state-of-the-art theory and design. Realistic experiments will require realistic simulation (though not necessarily duplication) of the actual flight conditions, which involves extending the state of the art for high enthalpy wind tunnels.

It is currently possible to determine the boundary-layer characteristics of a scramjet inlet in cold-flow tunnels (low enthalpy) which simulate Mach number and Reynolds number, and it is possible to test the combustor in present high enthalpy test facilities, e. g., shock tunnels. There are, however, very critical problems in the integration of these two components, such as the effect of the boundary layer at the combustor inlet on the combustion process, which require tests of a complete integrated model. In order to study the integrated unit experimentally, a facility must have adequate Mach number-Reynolds number capability at a sufficiently high stagnation temperature to permit spontaneous combustion in the combustor. Air must be used as the test gas, and sufficient run time must be available to ensure quasi-steady testing. Shock tunnels offer a capability for testing scramjet components and systems, but the available run time together with other operational problems combine to limit the usefulness of such a facility. Hotshot tunnels appear attractive for tests at high velocities, because of the long run time, relatively high total temperatures, and high total pressure.

A program is under way to evaluate the feasibility of using Tunnel F (Gas Dynamic Wind Tunnel, Hypersonic (F)) of the von Kármán Gas Dynamics Facility (VKF) (Refs. 1 and 2) for testing integrated scramjet models. Tunnel F is an arc-heated hypervelocity (hotshot) wind tunnel with 108-in. -diam test section (Mach 14 to 22) and a 54-in. test section (Mach 10 to 18). A useful run time of between 50 and 200 msec is attained. In terms of Mach number and Reynolds number, a wide range of flight conditions is simulated, using nitrogen as the test gas. The

results of a series of tunnel calibration tests using air as a test gas were reported in Ref. 3. It was demonstrated that clean (unvitiated) airflow could be generated at a stagnation temperature of 3000°K and stagnation pressures up to 10,000 psia. Current tunnel development programs (including an enlarged arc-chamber) are aimed at increasing this capability to 4000°K stagnation temperature at 20,000-psia pressure, or 2000°K at 40,000 psia.

A concurrent program was initiated to develop the instrumentation and theoretical tools necessary to obtain and analyze data during a test of a scramjet model in the tunnel. Such a program required a model with which the above development could be carried out. The results reported here were obtained in this development program.

A test program was initiated with an inclined flat plate model similar to the program reported in Refs. 4 and 5, in which hydrogen fuel was injected upstream of an inclined plate into a Mach 3 free stream (vitiated to raise the total enthalpy). The resulting fuel/air mixture passed through an oblique shock generated by the inclined plate, and the resulting temperature rise was sufficient to initiate combustion. However, when this test configuration was set up in the hypersonic tunnels (hotshot $M_\infty \approx 19$ and shock tunnel $M_\infty \approx 11$), the shock waves and wake generated by the injector assembly considerably modified the distribution of static pressure and heat-transfer rate on the surface of the inclined plate, even without fuel injection. Hence, the static temperature distribution behind the oblique shock would be an unknown and very nonuniform quantity. To overcome these obvious deficiencies, a double-oblique-shock model was developed such that fuel could be injected into a supersonic (as opposed to hypersonic) stream in the model combustor behind the second shock. The development of this model entailed a good deal of experimental research, thus the test program was conducted in the AEDC-VKF 16-in. shock tunnel I (Refs. 6 and 7). The 54-in. test-section of Tunnel F will be used in a subsequent test program.

The development of the model and results of aerodynamic performance tests are presented. The results of combustion tests, using this model, will be published in a subsequent report.

SECTION II
DESCRIPTION OF TUNNEL I AND TEST CONDITIONS

A photograph of the shock tunnel (I) is shown in Fig. 1, Appendix I. Discussions of this tunnel and its operating characteristics are given in

Refs. 6 and 7. Helium at room temperature and at pressures up to 13,000 psia is used to compress and shock heat the air in the driven tube. A double diaphragm separates the driver and driven sections. With this arrangement the driver and driven gas pressures may be accurately controlled before venting the gas from between the diaphragms to initiate the run.

The shock tube is operated in the tailored-interface mode at a primary shock Mach number of 3.83. The air is expanded through a 5-deg half-angle conical nozzle to a velocity of about 6700 ft/sec (free-stream Mach number 11). A schematic of the shock tunnel and shock tube notation is shown in Fig. 2. The driver and driven tube charge conditions and the resulting test section flow properties are summarized in Table I, Appendix II. The gas properties were computed using equilibrium thermodynamic properties of air (Refs. 8 through 10).

SECTION III
MODEL CONFIGURATIONS

3.1 SINGLE-OBLIQUE-SHOCK MODEL

A sketch of a flat plate model inclined at an angle of 35 deg and an airfoil injector installed in the shock tunnel is shown in Fig. 3a. The model was 6 in. long by 3 in. wide. The airfoil injector was located 15 in. upstream of the model. Figure 3b shows a 7-in. flat plate model attached to a 5-in. straight section (lower combustor plate) at an angle of attack of 25 deg.

3.2 DOUBLE-OBLIQUE-SHOCK MODEL

It was recognized that a double-oblique-shock inlet was an impractical device for efficient or even realistic total pressure recovery for a scramjet; however, the object of the test program was to develop a "simple" model in which supersonic combustion could be demonstrated and used for instrumentation development. Inviscid, two-shock theory calculations were carried out to determine adequate flow deflection angles for a model in the free-stream conditions given in Table I, Appendix II. These calculations indicated that a flow deflection angle of 25 deg should generate a compatible combination of static pressure, temperature, and Mach number in the combustor which should be adequate for spontaneous combustion of hydrogen as shown in Table II. Estimates of the ignition and reaction time were obtained from Ref. 11 and details of calculations are given in Appendix III.

A schematic of the model is shown in Fig. 4. It is desirable for the shock from the leading edge of the upper combustor plate (cowl) to impinge on the ramp-combustor intersection so that the Prandtl-Meyer expansion fan is cancelled by the shock wave. For this case the ramp angle, ramp length and the free-stream Mach number determine the position of the leading edge of the upper combustor plate and the channel height.

A model was fabricated with an inclined flat plate ramp section 3 in. wide and 7 in. long. These dimensions were a compromise based on obtaining a suitable combustor channel height (controlled by ramp length) for optical measurements but sacrificing plate width to prevent tunnel flow blockage. A combustor length of 5 in. was chosen which allowed the whole model to remain within the field of view of the schlieren system (the width is the same as for the inlet). The position of the upper combustor plate can be adjusted horizontally and vertically to provide some control of the capture area ratio and the point of intersection of the second shock relative to the inlet/combustor junction. A photograph of the model without its sidewalls installed in the test section is shown in Fig. 5. The junction of the inlet and combustor is a sharp corner as shown in Figs. 4 and 5; however, for some tests (during the analysis of flow separation at the junction) a round shoulder of 2-in. radius was used.

Significant static pressure decay was produced in the combustor of the model without sidewalls hence the majority of the development tests were carried out with sidewalls installed.

3.3 MODEL WITH SIDEWALLS

The model with sidewall windows added is shown in Fig. 6. The windows were of schlieren quality quartz, 0.25 in. thick, mounted in a steel frame. The position of the windows could be adjusted longitudinally. With side windows attached the combustor channel height was limited to nominal values of 0.3 and 0.5 in.

The leading edges of the quartz window frames were at an angle of 45 deg to the flow as shown in Fig. 7. Steel windows with a leading edge angle of 17 deg were also used. A boundary-layer scoop was used at the junction of the inlet and combustor for some runs. Later models had a 60-percent dense foam metal ramp as a boundary-layer bleed as shown in Fig. 8. The low leeward-side model pressures were used as a suction source to accomplish the boundary-layer bleed.

SECTION IV
INSTRUMENTATION

Heat-transfer measurements were made with slug calorimeters. The calorimeter consists of a thin-film platinum resistance thermometer deposited on an anodized aluminum disk as shown in Fig. 9a. Wall static pressures were measured with gage diaphragm pressure transducers. This type of pressure transducer consists of a semiconductor strain gage mounted directly on a thin metal diaphragm as shown in Fig. 9b. Pitot pressures were measured with quartz piezo gages.

Typical reservoir, test section pitot and model combustor exit pitot traces are shown in Fig. 10. Test data were taken during the period of constant pitot pressure. The upper trace corresponds to the reservoir (total) pressure (reflected shock region 5s in Fig. 2). The middle trace corresponds to the free-stream pitot (stagnation) pressure as measured by the pitot gage (p'_{O_∞}) shown on the side of the inlet in Fig. 8. It is shown that the tunnel achieves a uniform condition approximately 1 msec after the initial "starting" shock arrives, and the pitot pressure remains relatively constant for 2 or 3 msec. The bottom trace corresponds to the pitot pressure measured at the exit plane of the combustor. The combustor exit pitot gages may be seen through the sidewalls in Fig. 8. The start time of the combustor can be seen to be about the same as for the tunnel since the pitot pressure at the combustor exit achieves a relatively constant pressure about 1 msec after the beginning of the pressure rise.

SECTION V
EXPERIMENTAL RESULTS

5.1 STATIC PRESSURES AND HEAT-TRANSFER RATES ON THE FLAT PLATE RAMP

Static pressure and surface heat-transfer rates on the flat plate ramp at angles of attack of 35 and 25 deg are shown in Figs. 11 and 12. Data were obtained both with and without a diamond airfoil injector installed on the tunnel centerline approximately 15 in. upstream of the model leading edge.

The decay of static pressure along the ramp is the result of the combined effects of source flow and edge losses.

5.1.1 Source Flow Effects (Ref. 12)

The nozzle consists of a throat section with an exit radius of curvature that matches the slope of the 5-deg half-angle nozzle shown in Fig. 2. The nozzle flow, therefore, continues to expand in the test section, giving rise to gradients in the fluid-dynamic and state variables. An additional complication is introduced for a flat plate at angle of attack since the inclination of the plate to the free-stream velocity vector varies along the plate length. The variation in static pressure along the flat plate at each angle of attack (35 and 25 deg) attributable to source flow is shown in Figs. 11 and 12. The geometrical configurations used in these calculations are shown in Figs. 3a and 4. It is shown that the results are in good agreement for the 25-deg case, but there are additional factors contributing to the decay for the 35-deg case. The primary additional factor is edge losses.

5.1.2 Edge Effects

The pressure on the surface of the plate at angle of attack is higher than the free-stream pressure. Thus, without sidewalls, the gas is free to expand from the ramp. Since the gas flow on the plate is supersonic, a region of quasi-one-dimensional flow exists, having a boundary confined by the local Mach lines drawn from the tips of the plate as shown in Fig. 13. Only source flow effects should be evident in data taken within the boundary. The agreement of predicted and experimental values is good for the 25-deg case where the source flow effects predominate (Fig. 12). The 35-deg test data are obviously affected to a much larger degree by edge effects (see Fig. 11). Only the first two gages (see Fig. 13) are within the one-dimensional-flow boundary for the 35-deg test data.

The edge effects result in an outflow of gas from the open sides of the model, and this mass flow loss means that less fuel can be added to the flow before thermal choking occurs. In the case of a scramjet engine this mass loss could result in severe thrust losses (edge effects should not be present in axisymmetric inlets). The losses would of course be reduced if the angle of attack were reduced. The 25-deg test data indicate small edge losses; however, it must be remembered that this indication is confined to regions near the plate centerline.

The heat-transfer rate distributions shown in Figs. 11 and 12 indicate that the end of transition from a laminar to a turbulent boundary layer occurs about 3 in. from the leading edge of the plate. Based on current transition literature, the end of transition was expected to occur at approximately 6 or 7 in. The edge effect induces cross flows in the

boundary layer on the plate which may have contributed to the early transition. Theoretical values of turbulent heat-transfer rates were calculated from the relation given by Arthur (Ref. 13)

$$\dot{q}_{w,t} = 1.35 \frac{p_2^{0.8}}{X^{0.2}} \left\{\frac{U_2}{10^4}\right\}^{1.77} \left\{\frac{T_w}{10^2}\right\}^{-0.25} \left[0.9 - \frac{H_w}{H_o}\right] \qquad (1)$$

in which $\dot{q}_{w,t}$ is the turbulent heat-transfer rate (Btu/ft^2-sec), X is the distance from the leading edge (ft), p_2 is the oblique-shock value of the static pressure on the plate surface (lb/ft^2), T_w is the wall temperature (°R), U_2 is the velocity at the edge of the boundary layer on the plate (ft/sec), and H_w and H_o are total enthalpies evaluated at the wall and boundary-layer edge total temperatures (Btu/lb), respectively. At fixed angle of attack, U_2, T_w, H_w, and H_o are constants for a specific test condition and Eq. (1) is reduced to a function of X only (no account of the axial pressure gradient was included in the skin friction equation implicit in Eq. (1)).

Theoretical values of laminar heat transfer are given by:*

$$\dot{q}_{w\ell} \approx 0.332 \rho_\infty U_\infty (H_o - H_w) \sqrt{Re_{\infty_x}} \sqrt{p_2/p_\infty} \qquad (2)$$

where Re_{∞_X} is a Reynolds number per unit length based on free-stream conditions, and $\dot{q}_{w\ell}$ is the laminar heat-transfer rate (Btu/ft^2-sec). The derivation of this equation is given in Appendix IV.

The pressure and heat-transfer rate distributions on the 35-deg ramp were significantly altered (see Fig. 11) by the presence of the upstream injector even though no fuel was injected in any of the upstream injector runs. Disturbance of the hypersonic flow field by an injector upstream of the single-oblique-shock model (35-deg ramp) would make combustion test data very difficult to analyze. Therefore, the angle of attack was set to 25 deg and a combustor added to make a double-oblique-shock model in which fuel could be injected directly into the combustor.

Different ramp lengths on the model were used to determine whether tunnel blockage effects were present in the data shown in Fig. 12. Comparison of the data for ramp lengths of 7 and 9 in. indicates that tunnel blockage was not a significant factor.

---

*This correlation was suggested by J. D. Whitfield, ARO, Inc., Chief of the von Kármán Gas Dynamics Facility, AEDC.

5.2 MODEL WITHOUT SIDEWALLS

Static pressures measured in the combustor section without sidewalls (see Fig. 5) are shown in Fig. 14. Again, a pressure decay (parallel to the model centerline in Fig. 14a and perpendicular in Fig. 14b) was obtained because of mass flow loss from the open sides of the combustor. Oil droplet flow patterns (also shown in Fig. 14) taken during some of the tests confirmed that considerable outflow occurred both from the ramp and combustor. Thus the flow was not one-dimensional, and significant lateral gradients in fluid dynamic and state variables existed.

5.3 MODEL WITH SIDEWALLS

Sidewalls were installed on the model to reduce the mass flow losses in the combustor. The initial configuration tested is shown in Fig. 15a. The combustor channel height was approximately 0.3 in., and the leading edge of the sidewall windows was placed at the leading edge of the upper combustor plate. The model did not start during the useful run time of approximately 2 to 3 msec, and the static pressures did not achieve a uniform level. Schlieren motion pictures showed that the inlet boundary layer was separated and that a normal shock was standing at the combustor entrance. A number of variations in model configuration were investigated in an attempt to establish uniform, supersonic flow in the combustor. These tests are described below.

5.3.1 Effects of Increasing the Combustor Channel Height

The combustor channel height was increased from 0.3 to 0.5 in. to increase the ratio of inviscid flow height to boundary-layer thickness. In addition, the upper combustor plate (cowl) was moved back in order to maintain "shock on cowl lip" operation as shown in Fig. 15b. Steady, supersonic flow was established with this model configuration, and results are shown in Fig. 16a (square symbols). Comparison with the pressure ratio results in Fig. 14a obtained with the model without sidewalls shows that:

1. the pressure ratio near the entrance of the combustor was reduced from 0.0017 to 0.0008 with the model with sidewalls, and
2. the pressure ratio near the exit of the combustor was increased from 0.0007 to 0.0010.

The pressure ratio predicted by inviscid, two-shock theory is 0.00275, which is reduced by source flow effects to approximately 0.0020. Obviously,

additional pressure losses of considerable magnitude were present. The primary pressure loss mechanism is spillage and the effect of the boundary layer generated on the inlet modifying the interaction of the second shock from the cowl lip and the Prandtl-Meyer expansion fan at the sharp corner junction of the inlet and combustor. Based on inviscid, two-shock theory, the second shock must impinge exactly on the corner to cancel the Prandtl-Meyer expansion fan. When the combustor height was increased, it was necessary to move the upper combustor plate back, thus the second shock impinged behind the corner, downstream of the expansion fan. When a round shoulder was used, as shown in Fig. 15c, more of the flow was expanded before "seeing" the second shock, and an additional pressure loss was observed as shown in Fig. 16a (circular symbols). A secondary pressure loss mechanism is the interaction of the shock waves generated by the leading edge of the windows with the combustor entrance flow field. Results of tests with a combustor height of 0.5 in. and windows retracted to a position behind the junction of the inlet and combustor (as in configuration 15d) are shown as circles in Fig. 16b. Comparison of the pitot pressures measured at the combustor exit plane in Figs. 16a and b shows that the total pressure losses in the model flow field were significantly reduced with the windows retracted. Since a significant increase in the ratio of pitot pressure from 0.004 to 0.005 was obtained by retracting the window position, it was decided to reduce the combustor height to approximately 0.3 in. again in order to move the second shock back to the corner. The results of tests with this configuration (identical to Fig. 15e, with the boundary-layer bleed closed) are shown as triangles in Fig. 16b. Comparison of the pitot pressure ratios in Fig. 16b shows that a dramatic improvement in total pressure recovery was obtained. An increase in static pressure ratio from 0.0010 to 0.0015 was also obtained; however, even this value is substantially lower than the source flow corrected inviscid value of 0.0020. Additional variations in model configuration were tested in an attempt to increase the pressure ratio.

5.3.2 Effect of Window Leading-Edge Angle

The leading edge of the quartz window frames was at an angle of 45 deg (see Fig. 7a). At this angle and a ramp Mach number (M_2) of 3.5, a bow shock in the vertical plane perpendicular to the tunnel axis formed ahead of the window frames. This shock could not be directly observed because of the orientation of the model with respect to the schlieren system. To determine the effects of the window leading-edge angle, a series of tests was made using steel window blanks with a leading-edge angle of 17 deg. No bow shock should be formed at this angle. Two types of steel windows were used, a "sweptback" and a "square-type" (see Fig. 7). It was expected that the change to a smaller

leading-edge angle would improve model performance. The results shown in Fig. 17 indicate a decrease in model performance. The pitot pressure for the square steel windows was about 40-percent lower than for the quartz windows. The reason for this is not known.

5.3.3 Effect of Sidewall Position

Some tests were conducted to determine whether the position of the windows was a contributing factor in the sidewall effect on model performance.

Window position was measured from the sharp corner junction of the inlet and combustor, with the positive direction upstream of this location. The location of the leading edge of the windows had a marked effect on the pitot pressure measured at the exit plane of the combustor. The variation of combustor static and exit pitot pressures with window position is shown in Fig. 18, for sidewall windows with a leading-edge angle of 45 deg and window blanks with a leading-edge angle of 17 deg. The pitot pressure decreased as the window position was moved upstream. Note that the combustor height was 0.5 in. for the 45-deg leading-edge angle sidewalls and 0.3 in. for the 17-deg leading-edge angle sidewalls. The effect of sidewall position on the static pressure distribution is different for the two leading-edge angles; however, it is not known whether this is caused by the different angles or the combined influence of different channel height.

The results discussed in this and the previous section firmly established that the magnitude of the pressure losses is governed by the complicated flow field boundary-layer interaction at the combustor entrance. It is well known that boundary-layer separation phenomena are caused by the inability of the low momentum portion of the boundary layer to negotiate rapid changes induced by either shock waves or expansion waves. In an attempt to improve the pressure level and distribution in the combustor, some additional development tests were carried out in which part of the boundary layer was removed.

5.3.4 Ramp Boundary-Layer Control

A boundary-layer bleed was placed at the ramp combustor section corner as shown in Fig. 15e. The width of the bleed slot was varied from 0.020 to 0.080 in. The boundary-layer bleed had no significant effect on the model performance. Apparently the boundary layer was already separated before reaching the bleed.

A porous metal ramp (Figs. 8 and 15f) was found to be more effective in controlling the ramp boundary layer. Measured static and exit pitot pressures for the foam metal ramp are shown in Fig. 19. The

static pressure distribution was more uniform than for previous configurations. The pitot pressures were more consistent and repeatable.

Schlieren motion pictures showed that the separation shock at the intersection of ramp and combustor was much weaker in the tests with the foam metal ramp model. A schematic of the combustor entrance flow field for the solid and porous ramp tests is shown in Fig. 20. The 60-percent dense foam metal provides continuous boundary-layer suction, utilizing the pressure differential between the ramp surface and the evacuated interior of the model. It was estimated that 0.5 percent of the ramp mass flow was removed through the porous ramp. The improvement in inlet pressure recovery was attributed to the fact that the low momentum portion of the boundary layer was removed, which improves the stability of a boundary layer.

SECTION VI
DISCUSSION AND SUMMARY OF EXPERIMENTAL RESULTS

The effects of the various changes in model configuration on the combustor exit pitot pressure and Mach number are summarized in Fig. 21. The highest pitot pressure recovery was obtained with a combustor height of 0.3 in. for which the second shock impinged close to the "sharp" corner. This corresponds to the most effective cancellation of the Prandtl-Meyer expansion fan by the compression shock. Complete cancellation could not be obtained primarily because of the boundary layer and secondarily because of mechanical difficulties in assembly and alignment. Of the configurations having the highest pressure recovery, the porous ramp was the better of the two because of the more uniform static pressure in the combustor. This is shown in Fig. 22. Also shown in Fig. 22 are the ramp pressures, two-shock theory level, and the open sidewall model data to show the marked improvement in overall model performance. The uniform level of the static pressures in the combustor with the porous ramp model should make interpretation of the pressure data for tests with injection easier than with the other configurations.

The data in Fig. 22 illustrate that although an improvement in pressure level and uniformity has been obtained, there is approximately a 50 percent difference in the inviscid two-shock theory level and the experimental values from tests with the porous ramp model. This difference could be caused by a number of factors, among them the following:

1. Three-dimensional flow effects caused by the low aspect ratio of the ramp (edge losses) and by tunnel source flow.
2. Viscous effects (boundary-layer displacement and momentum losses).
3. Oblique-shock-boundary-layer interactions.
4. The complex interaction between the inviscid and viscous flow field at the intersection of the ramp and combustor.

The pressure decay caused by source flow effects on the ramp accounts for a drop of static and pitot pressure level in the combustor of approximately 22 and 15 percent, respectively.

Investigation of schlieren motion pictures (see Fig. 20) indicated that relatively weak shocks were present in the combustor flow. Thus the primary pressure loss mechanism is thought to be caused by interactions at the combustor entrance.

The static and pitot pressures are apparently strongly influenced by the abrupt exit expansion as shown by the decrease in pressure ratios measured at the combustor exit in Fig. 19. The measured values at the exit are approximately $p_3 \approx 11$ psia and $p'_{o,3} \approx 68$ psia, and the estimated corresponding total pressure is $p_{o,3} \approx 107$ psia (assuming $\gamma \approx 1.3$). The average measured value of static pressure in the combustor is ≈13.5 psia. Assuming the flow near the combustor exit undergoes an isentropic expansion from 13.5 to 11 psia, which increases the flow Mach number (the expansion could be caused by a decrease in boundary-layer thickness, because of a base pressure effect, and hence an increase in inviscid flow area) then the average combustor pitot pressure can be calculated. The ratio of static to total pressure at the combustor exit is used as an entry point in isentropic expansion tables. The ratio of average static to total pressure in the combustor is used to determine the new position in the tables to obtain the ratio of average static to pitot pressure in the combustor. The average pitot pressure can then be obtained from this ratio and the measured static pressure. Thus the average combustor pitot pressure is $p'_{o,3} \approx 74$ psia.

The estimated static temperature in the combustor is ≈1200°K, using Mollier data and assuming adiabatic flow. Heat transfer to the model, based on experimental values of heat-transfer rate, is approximately 5 percent of the total enthalpy; thus the assumption of adiabatic flow is realistic. A Mollier diagram of the theoretical and measured performance is shown in Fig. 23. The poor performance of a two-shock inlet is illustrated by the difference between the isentropic and inviscid

two-shock states. When viscous effects are added as in the experimental case, the total pressure losses can be prohibitively large.

SECTION VII
COMBUSTION CONSIDERATIONS

The ignition delay and reaction times calculated using Eqs. (III-1) and (III-2) in Appendix III and the average static pressure and temperature of 13.5 psia and 1200°K are, respectively:

$$\left.\begin{aligned} \tau_{ID} &\approx 25\ \mu\text{sec} \\ \tau_{R} &\approx 27\ \mu\text{sec} \end{aligned}\right\} \quad \begin{aligned} &\text{fuel/air premixed} \\ &\text{hydrogen fuel} \end{aligned}$$

Thus the time required for complete reaction is approximately double that estimated for two-shock theory performance shown in Table II. In combustion experiments, the hydrogen fuel will not be premixed and will also be at 300°K, which will cool the air below 1200°K. For example, for an overall equivalence ratio of 0.2 the mixture temperature will be 1130°K, resulting in $\tau_{1D} \approx 41.3\ \mu$sec and $\tau_{R} \approx 29\ \mu$sec; thus the time required for complete combustion will then be approximately three times the two-shock theory estimate. This means that the length required for combustion of the fuel will be increased from 1.5 in. (L_o in Table II) to at least 4.5 in., with an unknown length to be added for mixing of the fuel and air. The length of model combustor available for both mixing and combustion is ≈4 in. since 1 in. of combustor length is necessary for installation of the plenum chamber for the hydrogen injection. It is interesting to note that an estimated small increase in static temperature above the two-shock theory level (1160°K, see Table II) was obtained in the experiments.

It is obvious that the current performance is rather marginal for combustion testing, hence a heater will be installed on the driver tube of the shock tunnel to increase the total enthalpy and the static temperatures throughout the flow field.

SECTION VIII
CONCLUSIONS

Development of a scramjet model at AEDC has yielded the following conclusions:

1. A double-oblique-shock scramjet has been developed with which it should be possible to do supersonic combustion tests.
2. The measured pressure levels (combustor pitot and static) are approximately 50 percent less than the values predicted for inviscid two-shock performance.
3. The pressure losses (combustor pitot and static) are attributed to two main causes:
   a. Source flow effects in the conical tunnel nozzle generate a decay in static pressure on the inclined flat plate inlet leading to a pressure level in the combustor approximately 22 percent below the two-shock theory level.
   b. Spillage at the combustor inlet and inviscid-viscous flow interactions between the boundary layer on the ramp, the second shock from the cowl lip, and Prandtl-Meyer expansion at the junction between the inlet and combustor are the major contributors to the additional reduction in pressure level in the combustor of approximately 28 percent.
4. Combustion testing with this model would lead to only partial combustion within the combustor because of the large static pressure losses, hence the total enthalpy of the flow is to be increased by heating the shock tunnel driver section.
5. The highest pressure recovery coupled with a uniform pressure distribution was obtained with a porous inlet ramp and a model configuration in which the shock from the cowl lip impinged closest to the junction of the inlet and combustor. This configuration allows the most effective cancellation of the Prandtl-Meyer expansion at the junction.

REFERENCES

1. Ball, H. W. "Calibration of the 100-inch Hypervelocity Tunnel F." AEDC-TDR-63-46 (AD298279), March 1963.
2. Griffith, B. J. and Weddington, E. D. "Recent Refinements and Advancements of Hypersonic Testing Techniques in the 100-inch Tunnel F of the von Karman Gas Dynamics Facility." Arnold Engineering Development Center, Proceedings of the Fourth Hypervelocity Techniques Symposium, November 15-16, 1965.
3. Osgerby, I. T. and Smithson, H. K. "Operation of AEDC-VKF 100-inch Hotshot Tunnel F with Air as a Test Gas and Application to SCRAMjet Testing." AEDC-TR-67-242 (AD664906), December 1967. Presented at the Fifth Hypervelocity Techniques Symposium, University of Denver, Colorado, March 1967.

4. Rhodes, R. P., Rubins, P. M., and Chriss, D. E. "The Effect of Heat Release on the Flow Parameters in Shock-Induced Combustion." AEDC-TDR-62-78 (AD275366), May 1962.

5. Rubins, P. M. and Rhodes, R. P. "Shock-Induced Combustion with Oblique Shocks, Comparison of Experiment and Kinetic Calculations." AEDC-TDR-63-103 (AD405887), June 1963. AIAA Journal, Vol. I, No. 12, pp. 2778-2784, December 1963.

6. Ball, H. W. "Initial Operation of the Pilot Counterflow Test Unit (I)." AEDC-TR-65-132 (AD465893), July 1965.

7. Haun, J. H. and Ball, H. W. "Calibration of the Shock Tunnel Component of Counterflow Range (I) at Mach 7.5." AEDC-TR-66-64 (AD632816), May 1966.

8. Hilsenrath, J. and Klein, M. "Tables of Thermodynamic Properties of Air in Chemical Equilibrium Including Second Virial Corrections from 1500°K to 15,000°K." AEDC-TR-65-58 (AD612301), March 1965.

9. Grabau, M. and Brahinsky, H. S. "Thermodynamic Properties of Air from 300 to 6000°K and from 1 to 1000 Amagats." AEDC-TR-66-247 (AD646172), January 1967.

10. Lewis, C. H. and Burgess, E. G., III. "Charts of Normal Shock Wave Properties in Imperfect Air." AEDC-TDR-64-43 (AD433958), March 1964.

11. Pergament, H. S. "A Theoretical Analysis of Non-Equilibrium Hydrogen-Air Reactions in Flow Systems." AIAA-ASME Hypersonic Ramjet Conference, Naval Ordnance Laboratory, White Oak, Maryland, Paper No. 63113, April 1963.

12. Whitfield, Jack D. and Norfleet, Glenn D. "Source Flow Effects in Conical Hypervelocity Nozzles." AEDC-TDR-62-116 (AD276124), June 1962.

13. Arthur, P. D., et al. "Flat Plate Turbulent Heat Transfer at Hypervelocities." J. Spacecraft and Rockets, Vol. 3, No. 10, p. 1549, October 1966.

APPENDIXES

I. ILLUSTRATIONS
II. TABLES
III. IGNITION DELAY AND REACTION TIME
IV. LAMINAR HEAT-TRANSFER CORRELATION

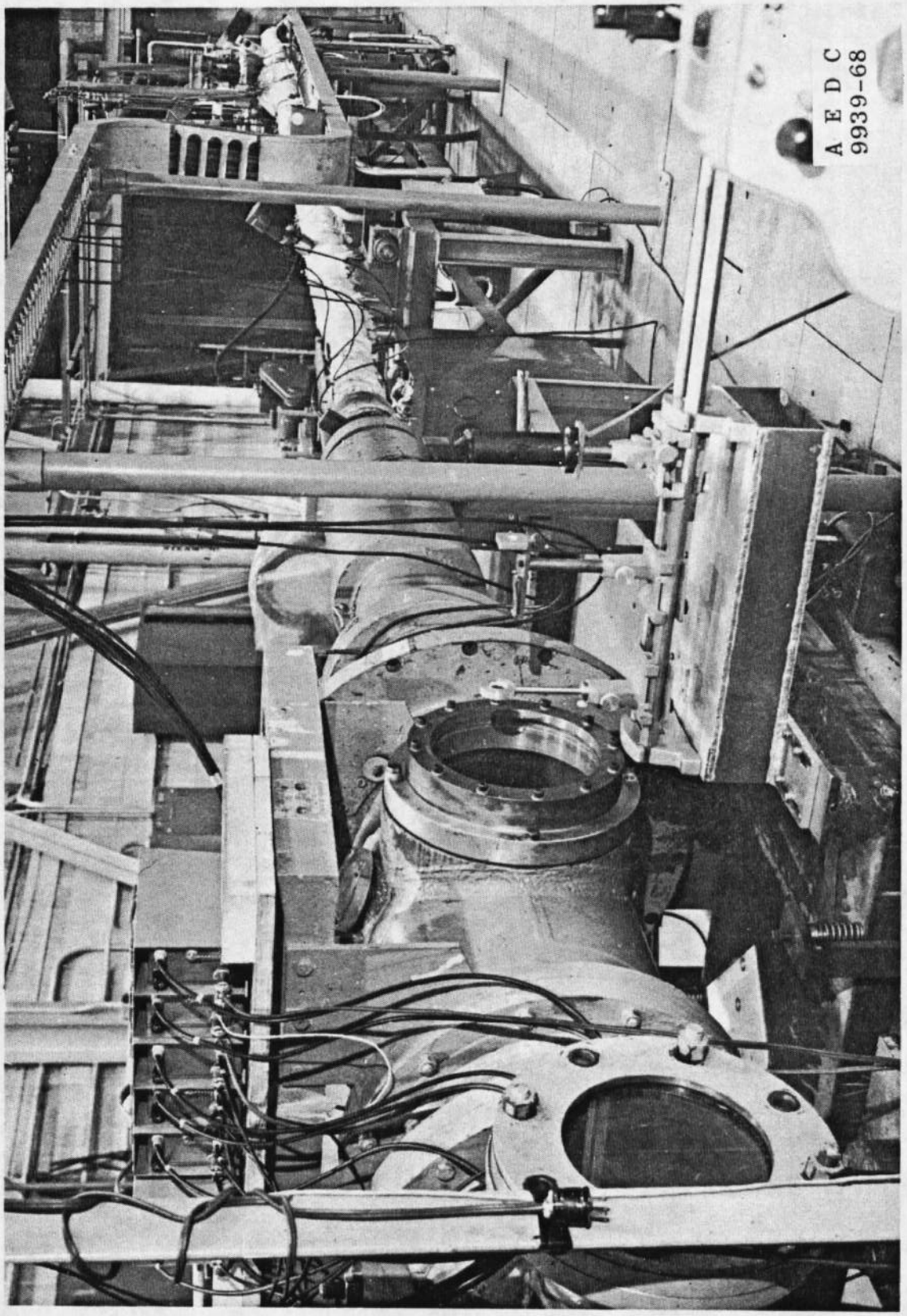

Fig. 1 Photograph of Tunnel I

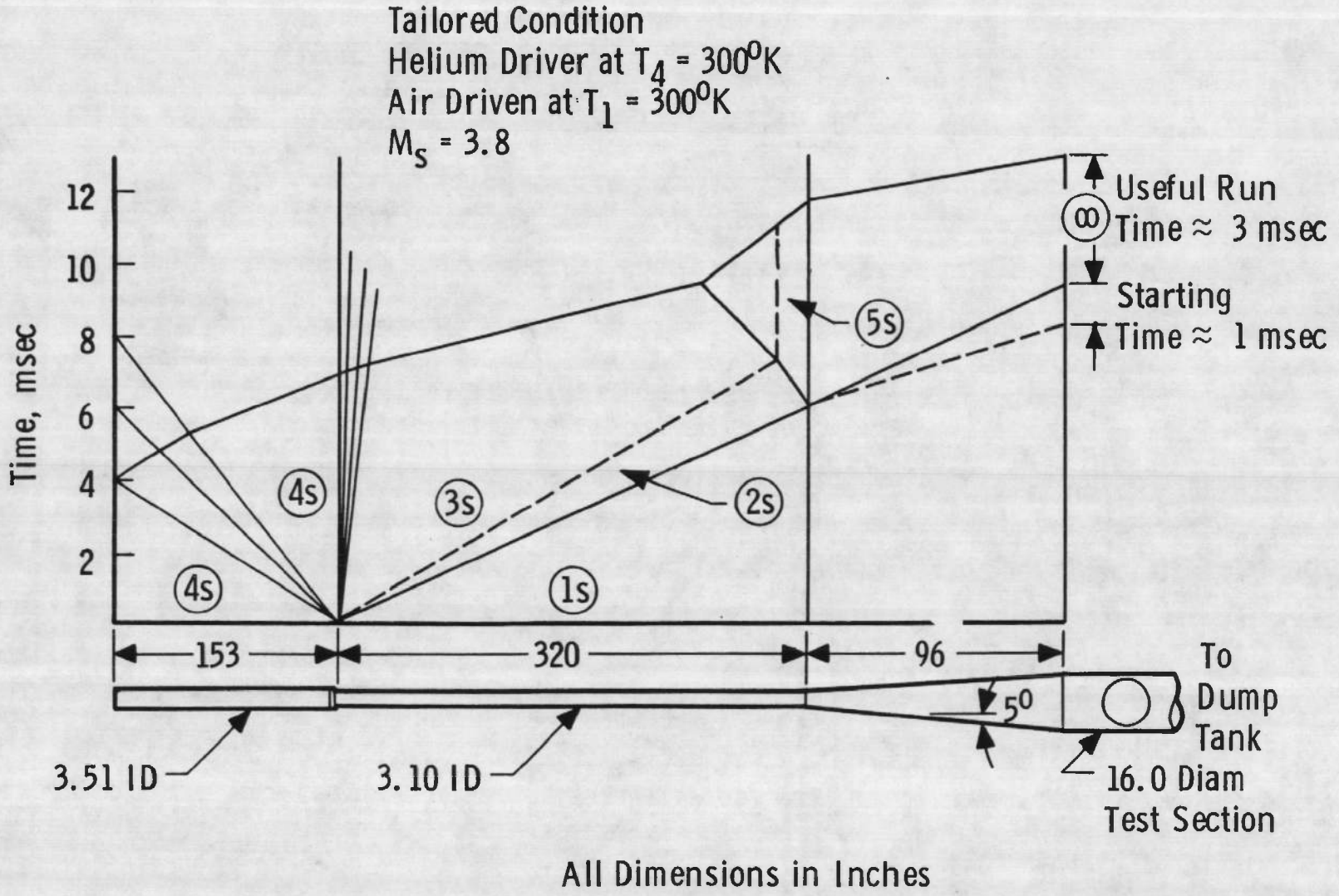

Fig. 2 Time-Distance Diogrom for Shock Tunnel I

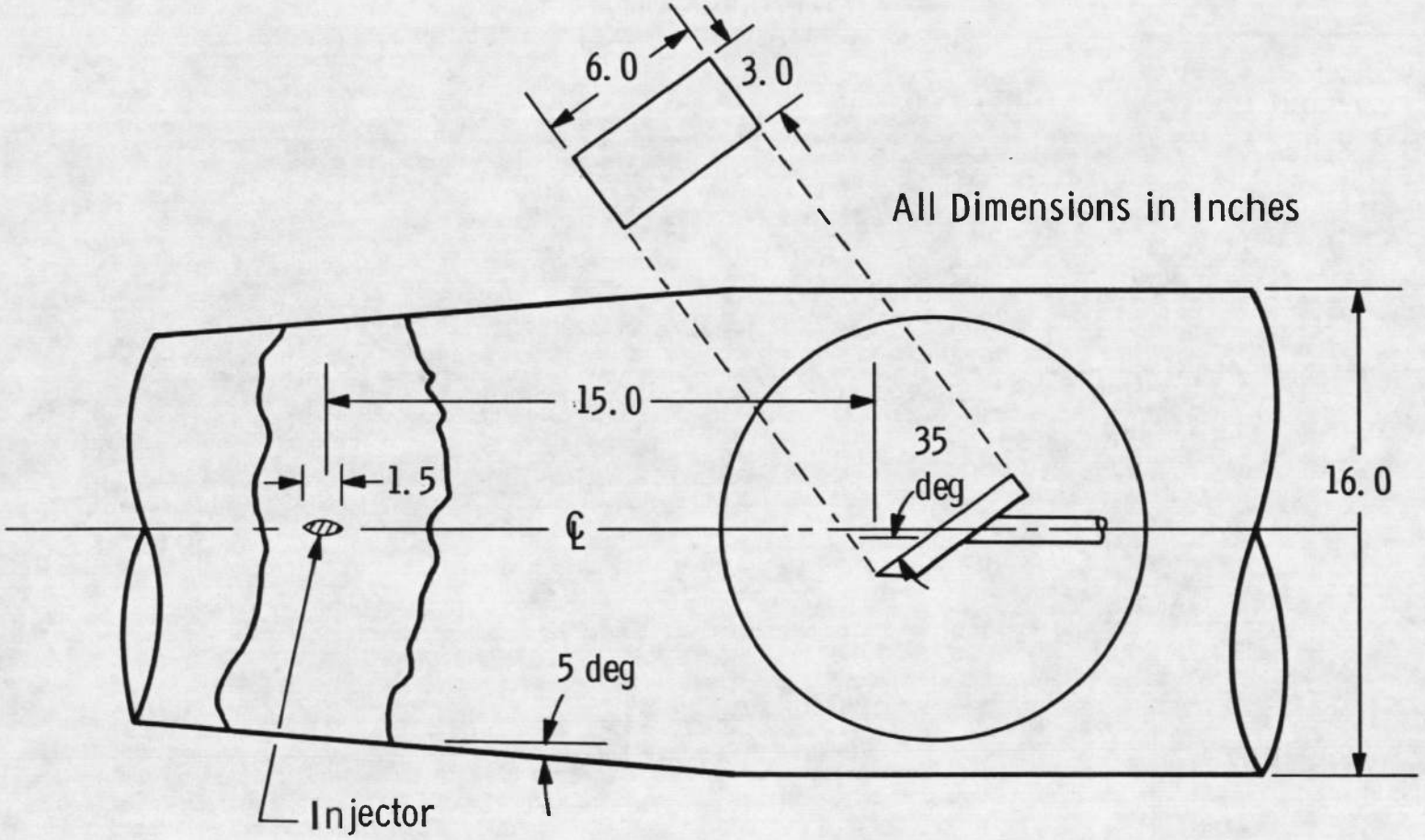

a. Inclined Flat Plate Model at 35 deg

Fig. 3 Flat Plate Models

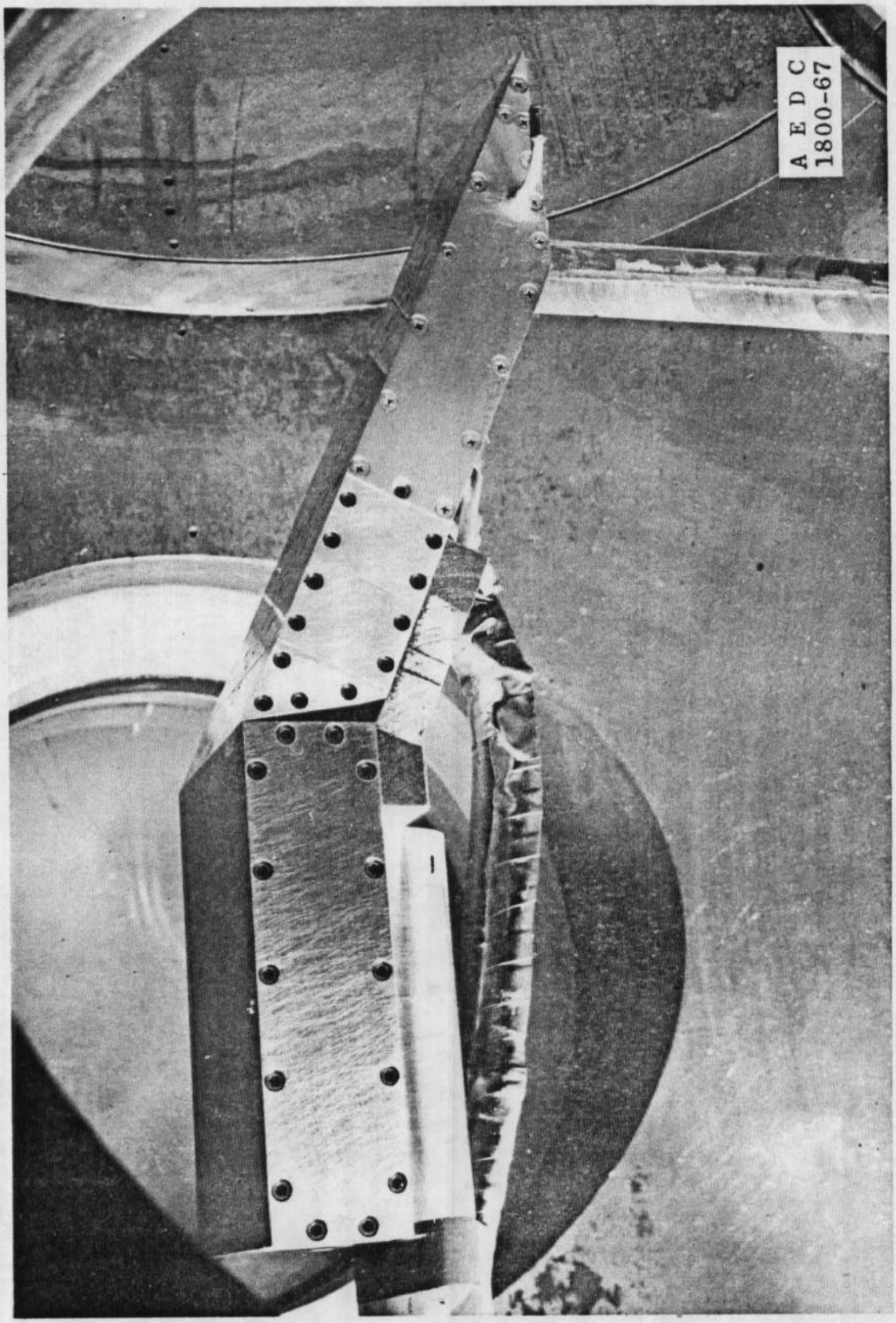

b. Inclined Flat Plate Model at 25 deg

Fig. 3 Concluded

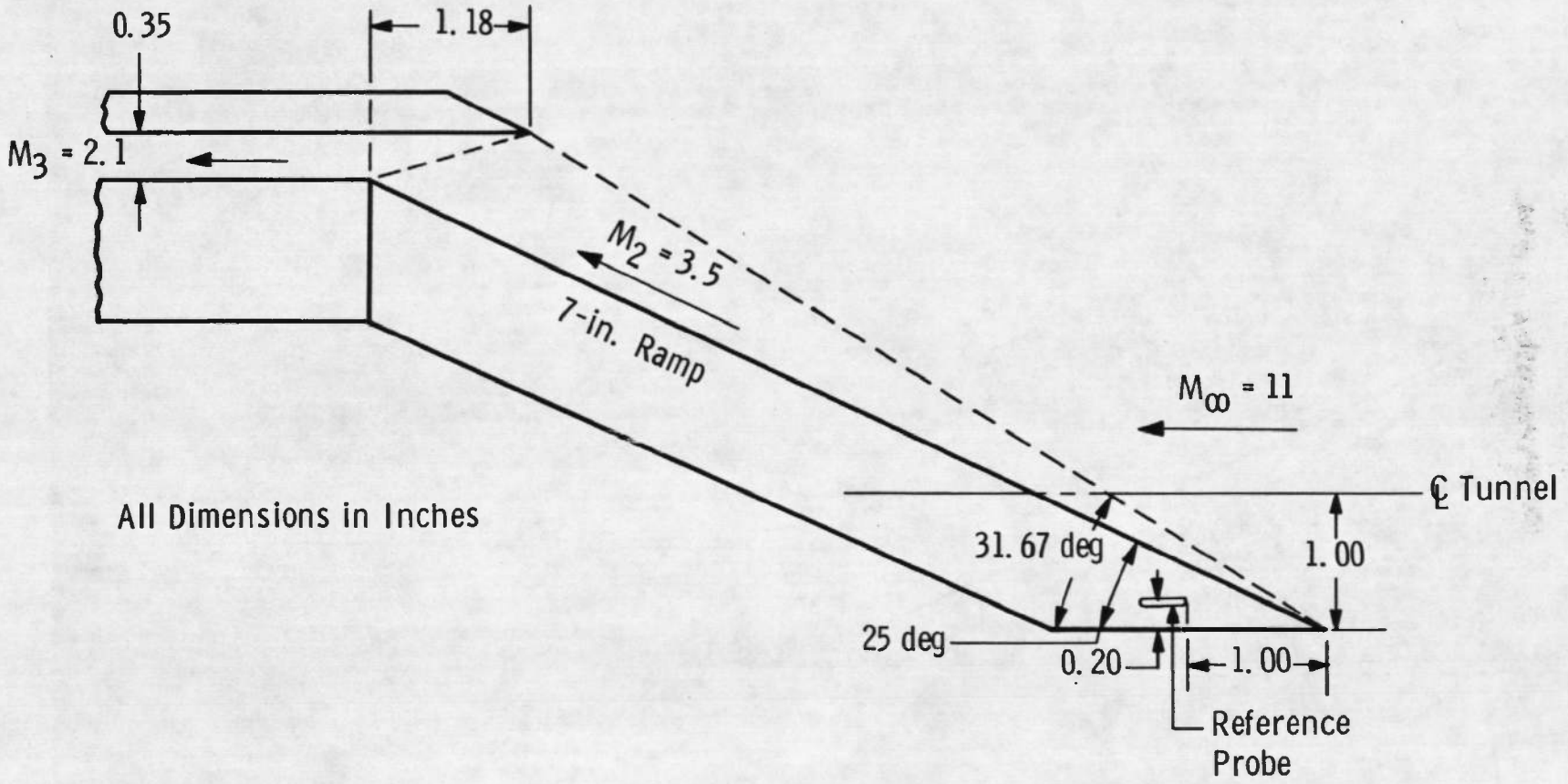

Fig. 4 Design Dimensions for the Ramp at 25 deg (M_∞ = 11)

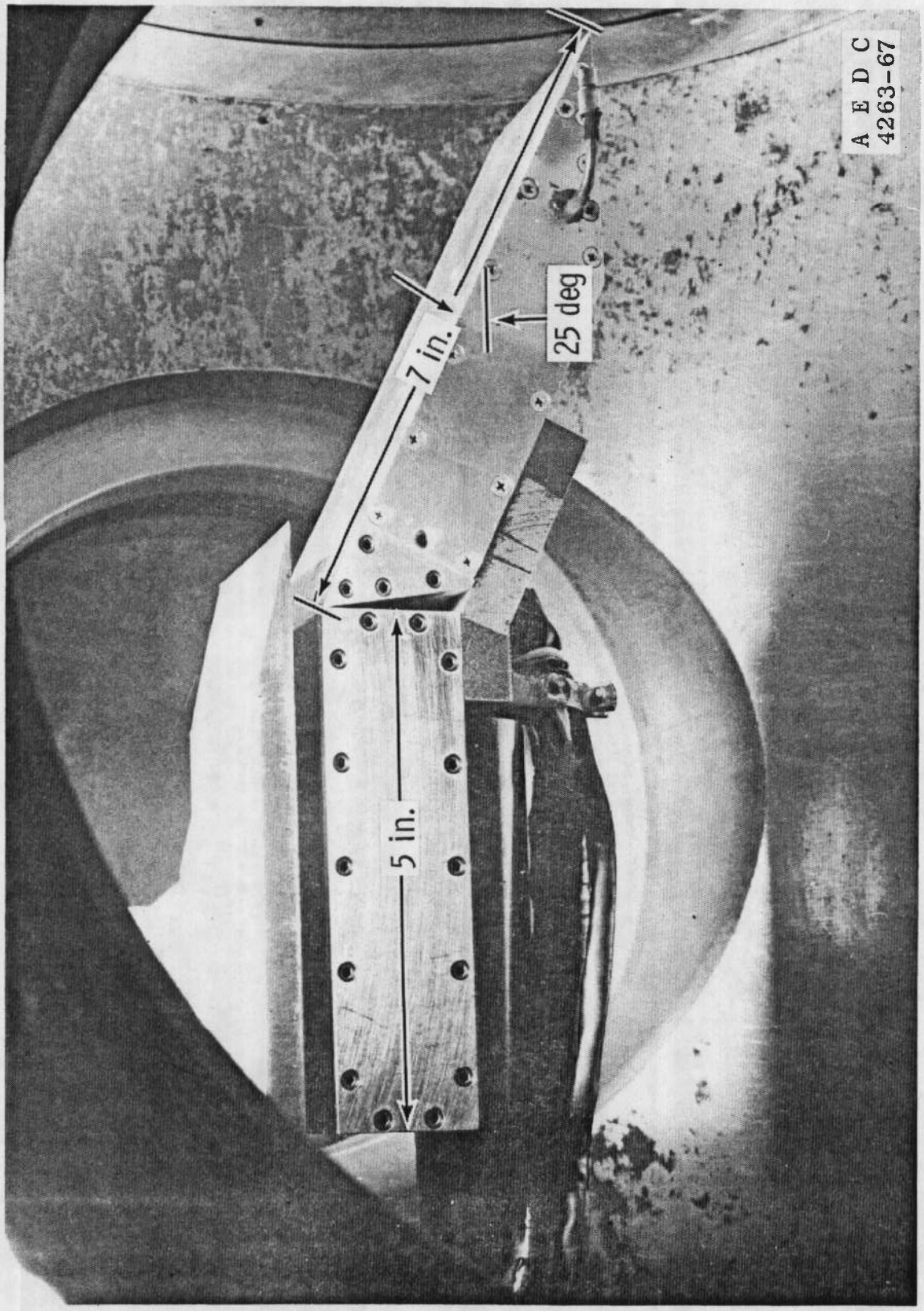

Fig. 5 Model without Sidewalls

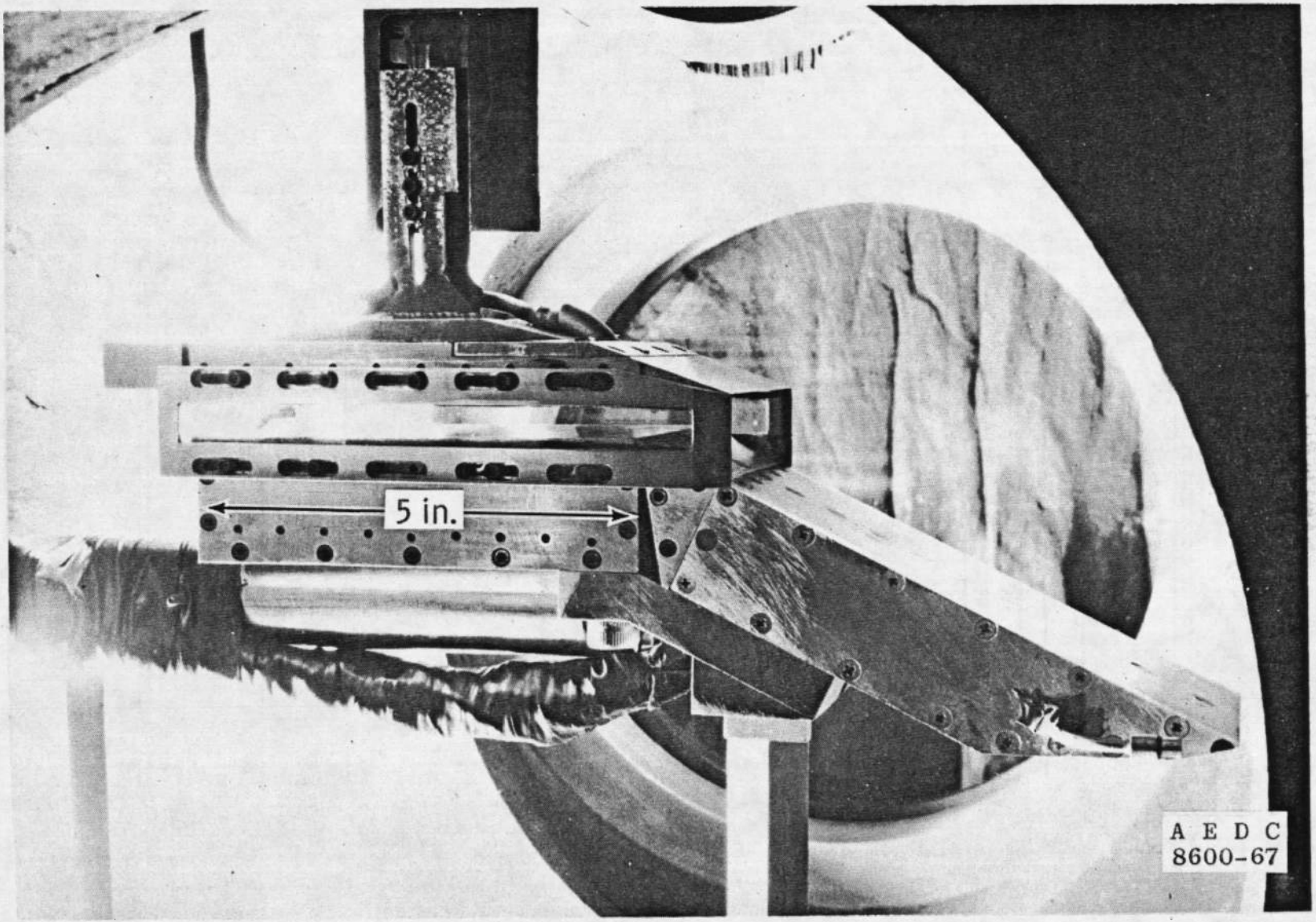

Fig. 6 Model with Sidewalls

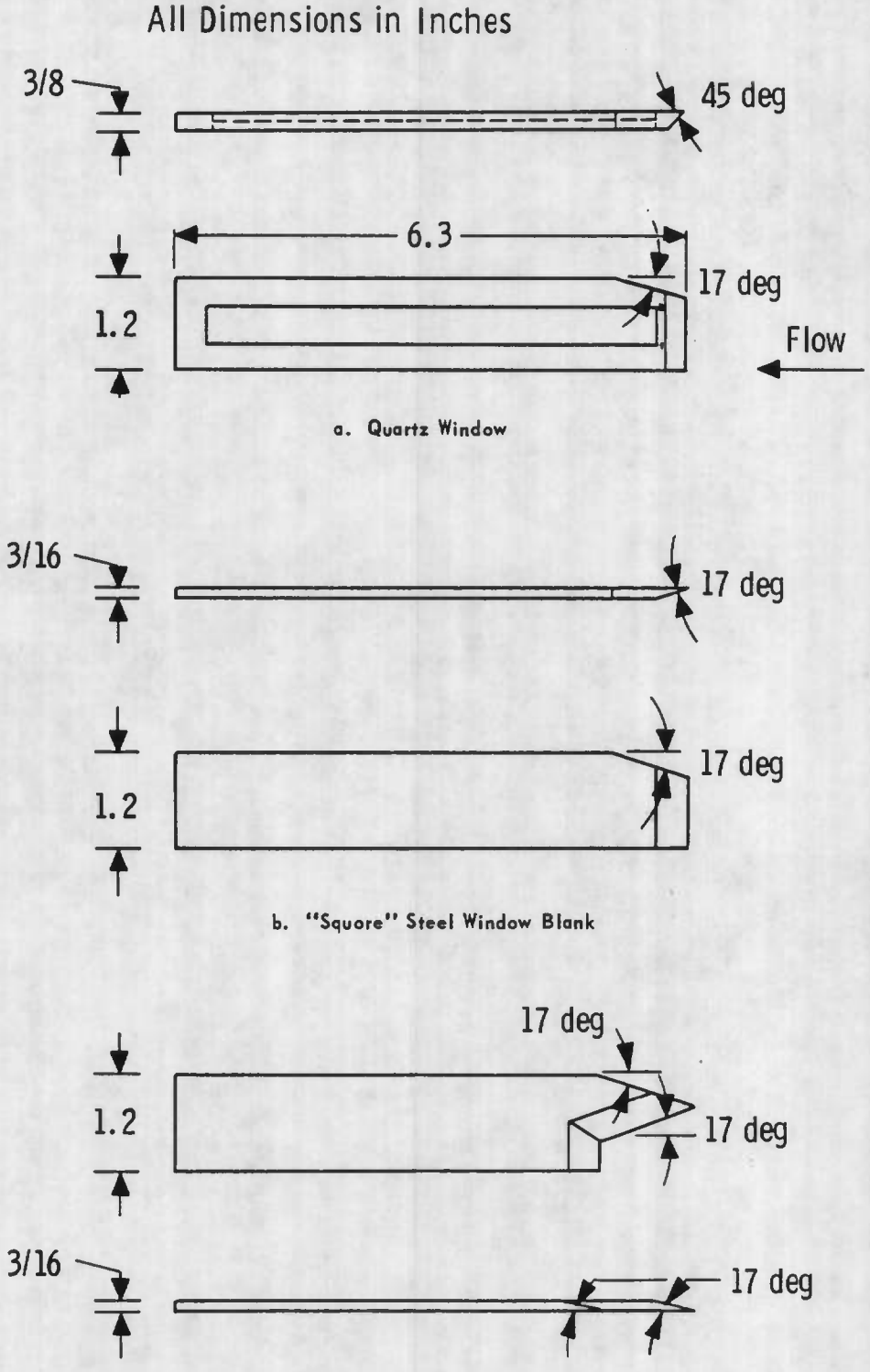

a. Quartz Window

b. "Squore" Steel Window Blank

c. Swept Back Window Blank

Fig. 7 Sidewall Window Configurotions

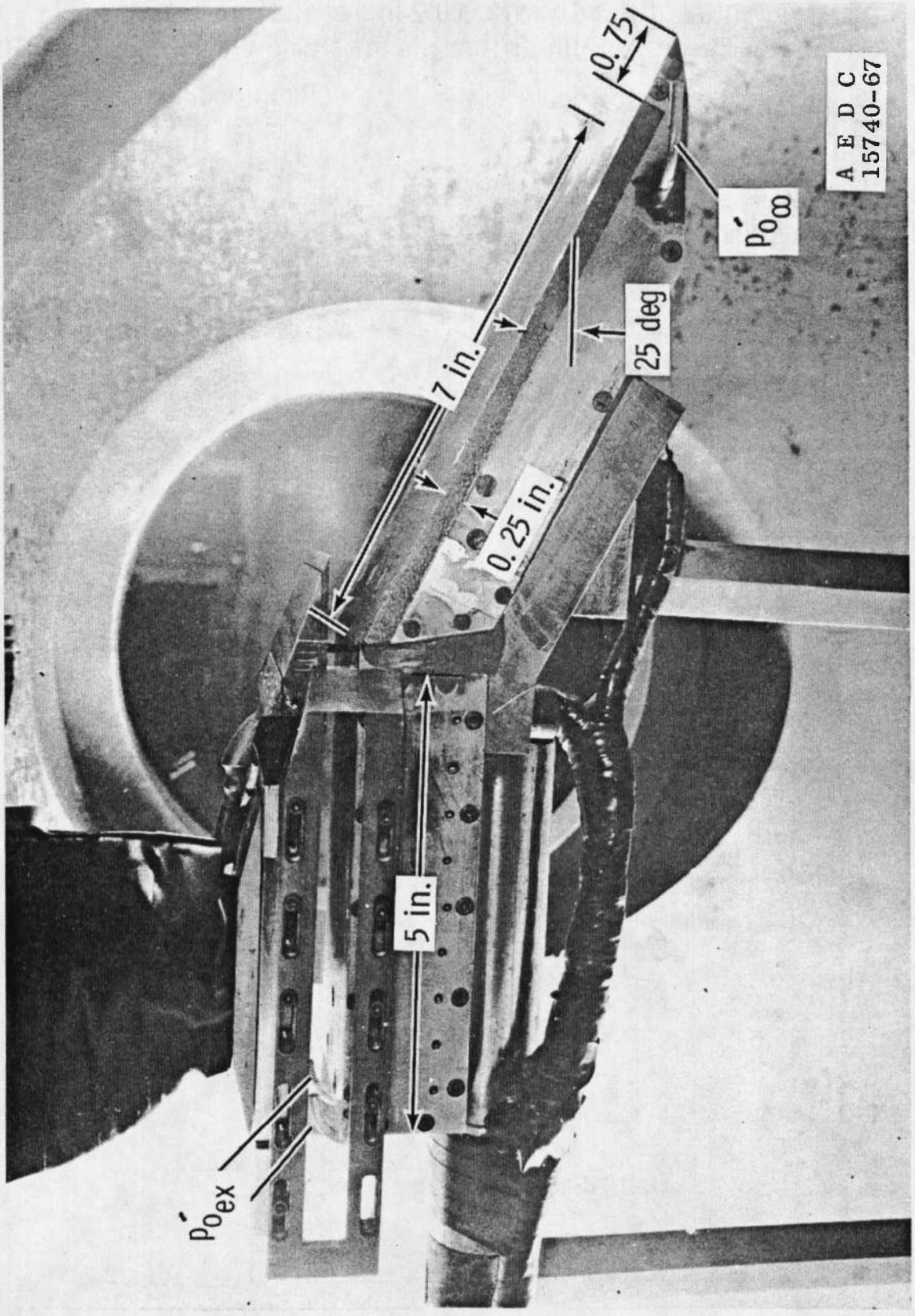

Fig. 8 Model with Foam Metal Ramp

Note: There is an insulating layer (0.00012 in.) of aluminum oxide (Al_2O_3) between the platinum film and the aluminum disk.

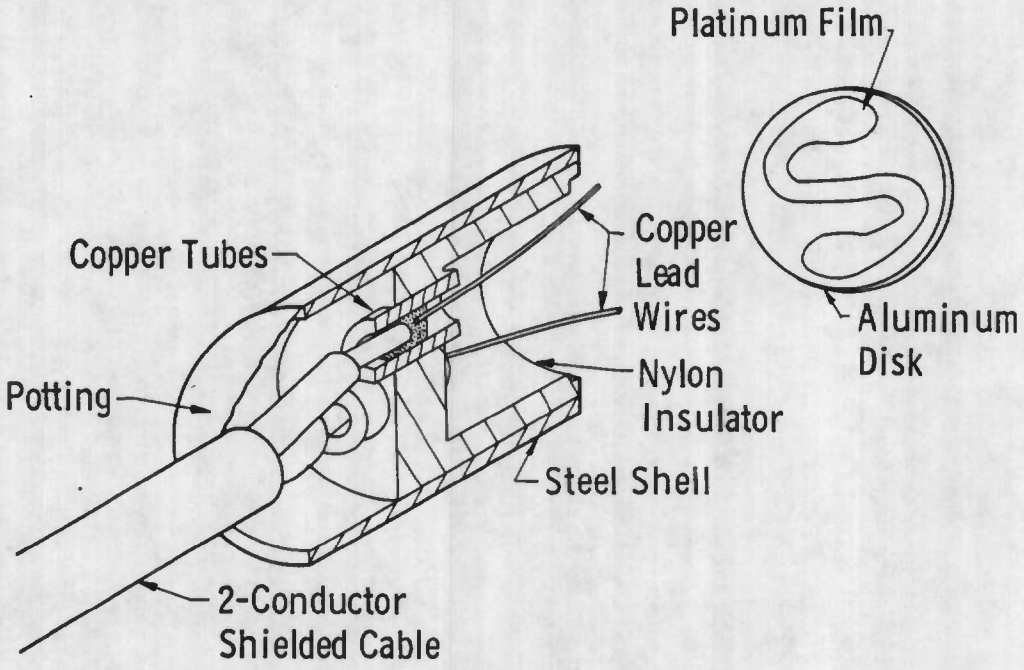

a. Slug Calorimeter with Thin-Film Resistance Thermometer Temperature Sensor

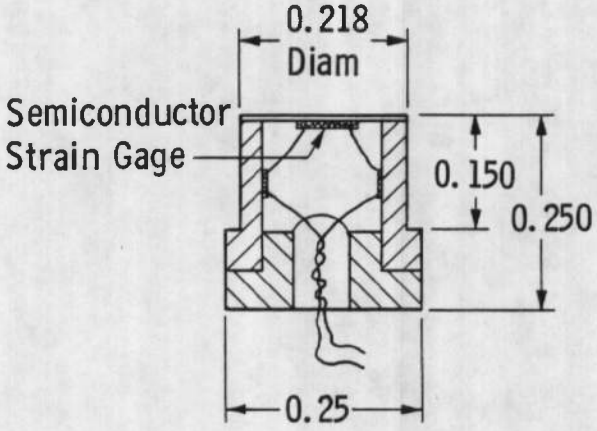

G.D. (Gage-Diaphragm)

b. Pressure Gage

Fig. 9 Heat-Transfer and Pressure Transducers

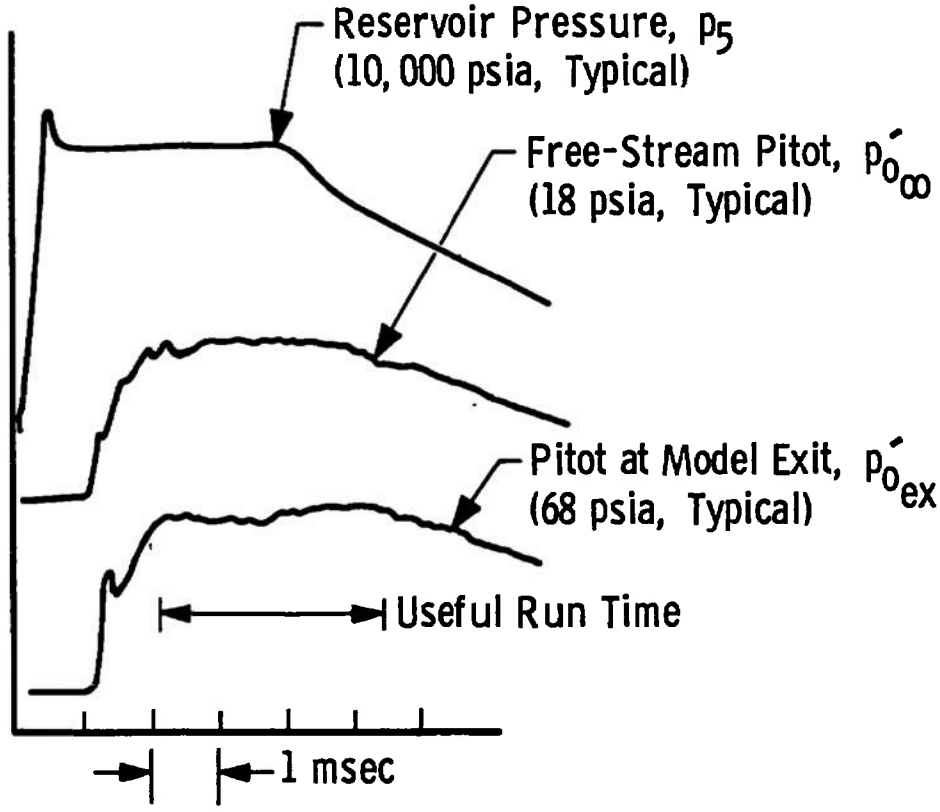

Fig. 10 Typical Pressure Traces

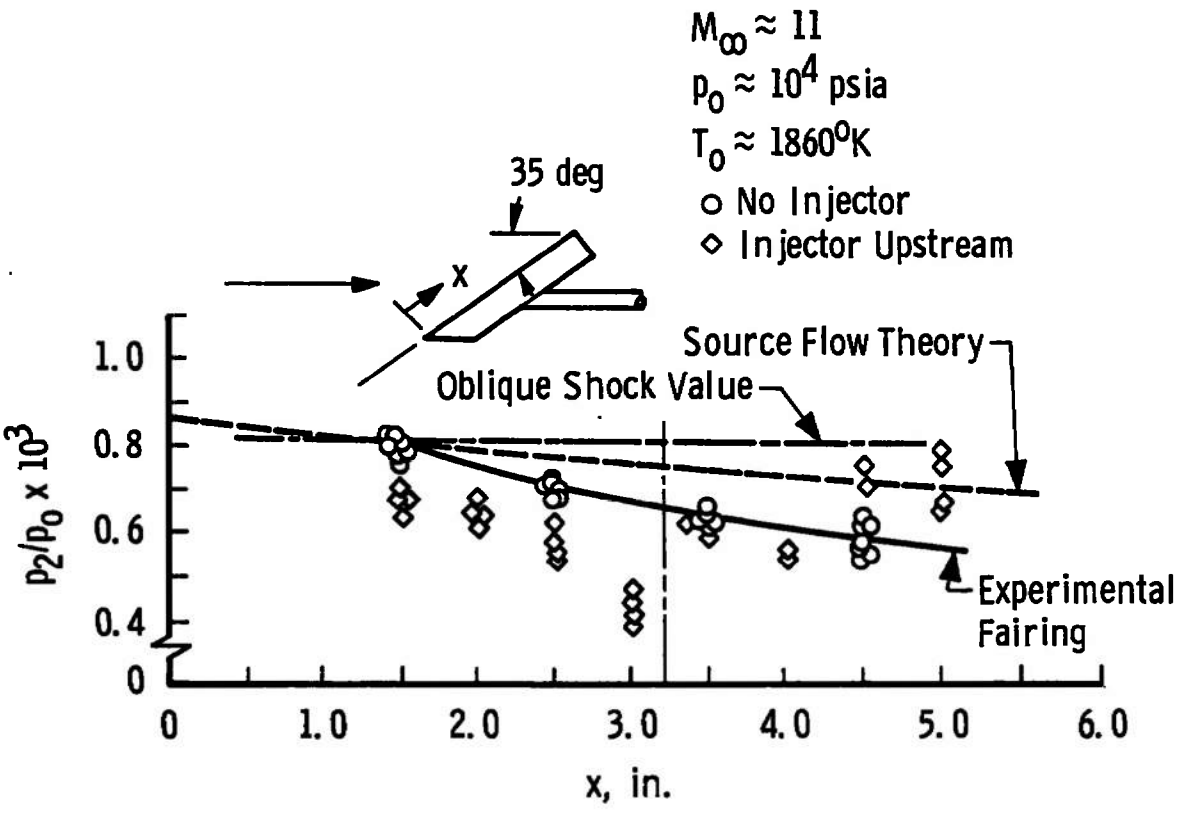

a. Static Pressure

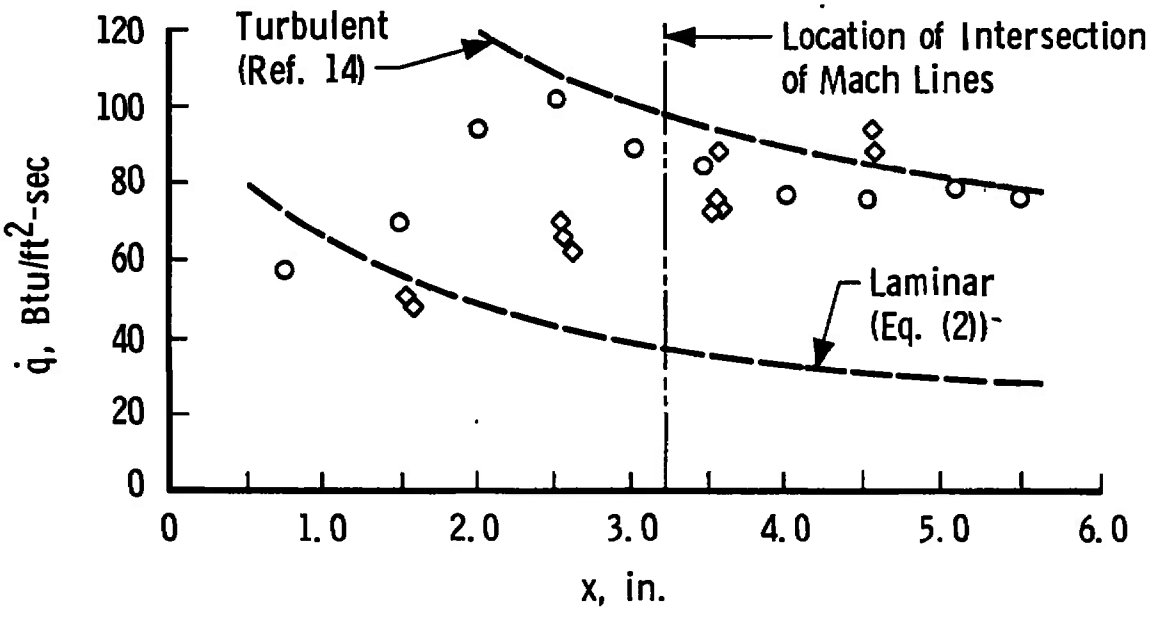

b. Heat-Transfer Rates

Fig. 11 Static Pressures and Heat-Transfer Rates on the Flat Plate Ramp at 35 deg

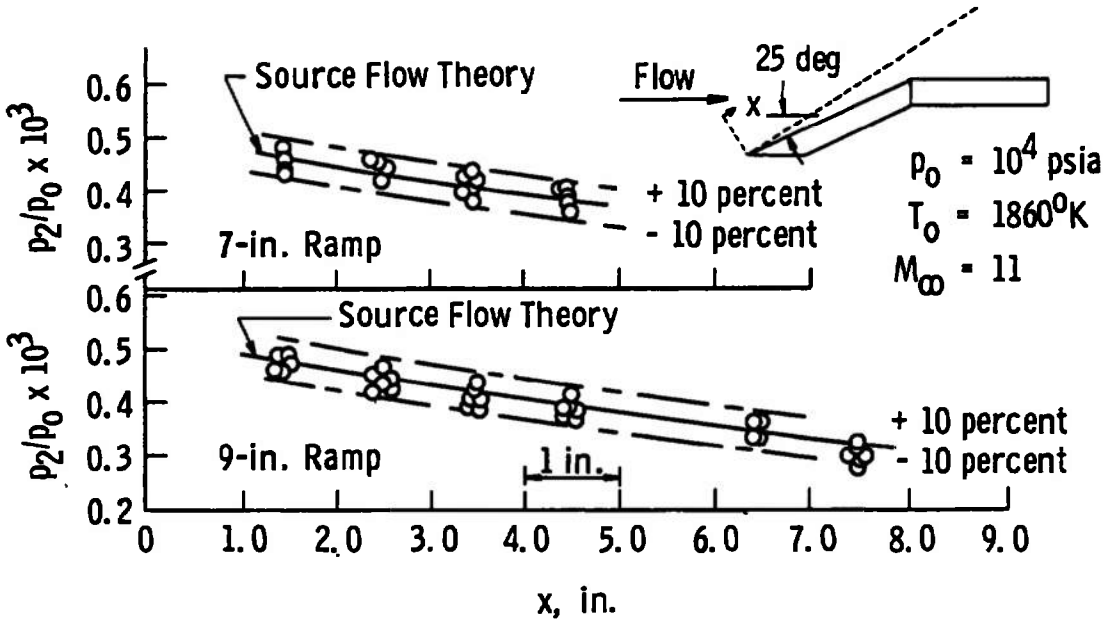

a. Static Pressure

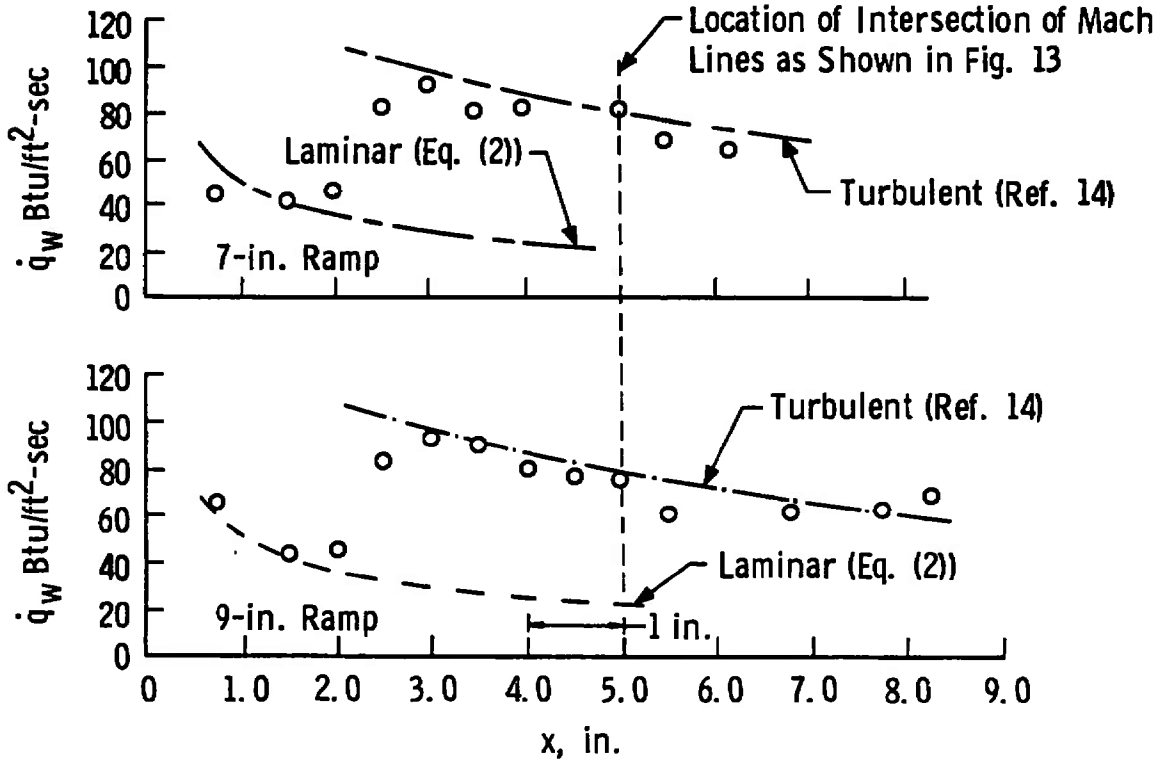

b. Heat-Transfer Rates

Fig. 12 Static Pressure and Heat-Transfer Rates on the Flat Plate Ramp at 25 deg

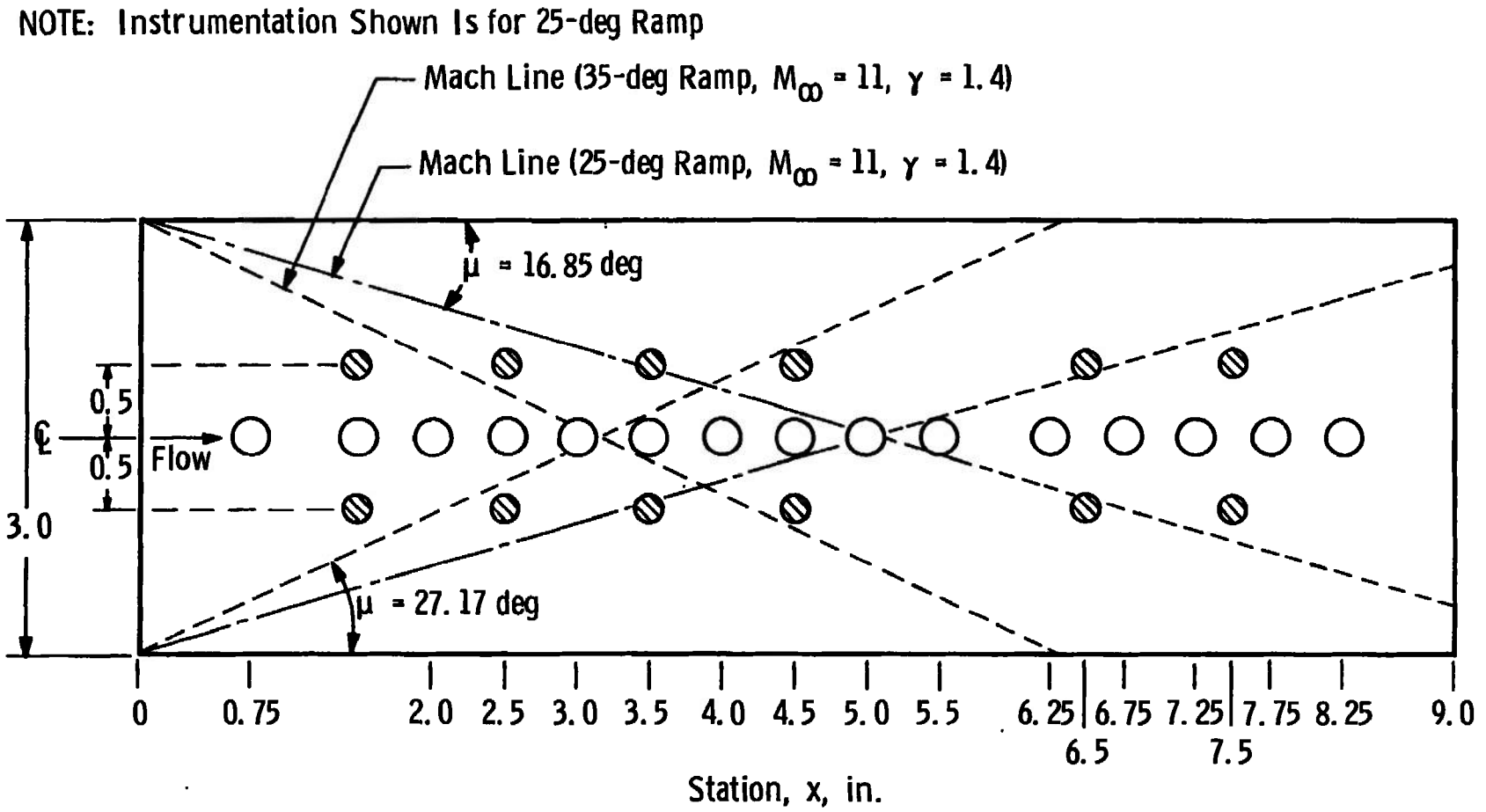

Fig. 13 Ramp Instrumentation Location and Flow Regions

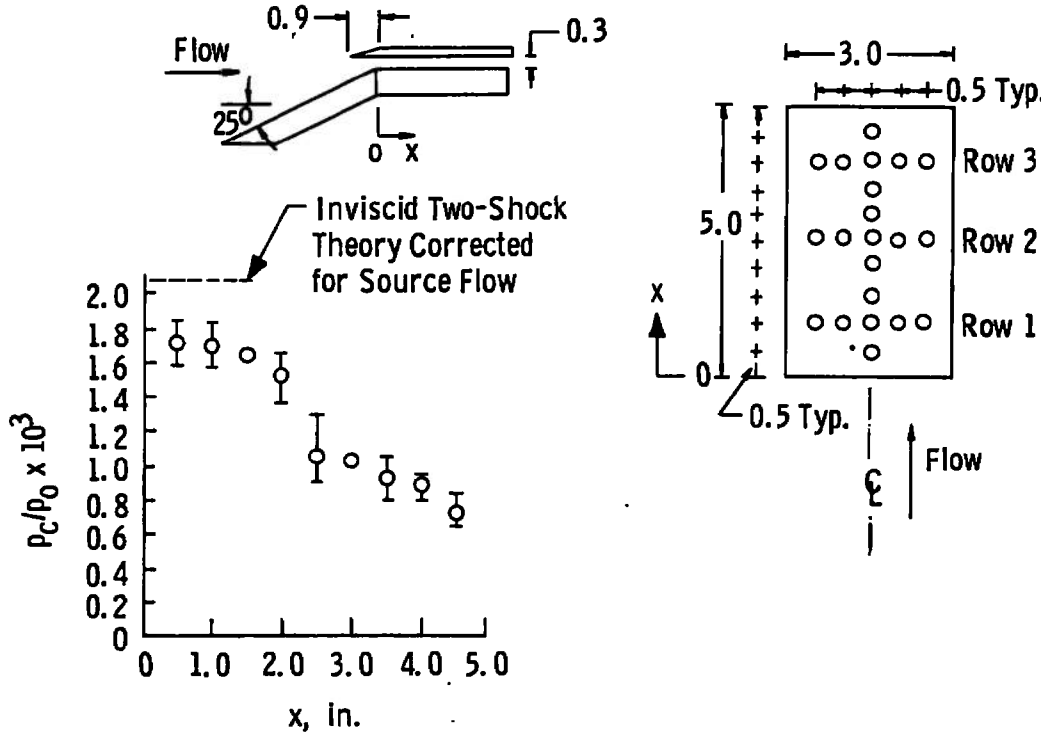

a. Along Model Centerline

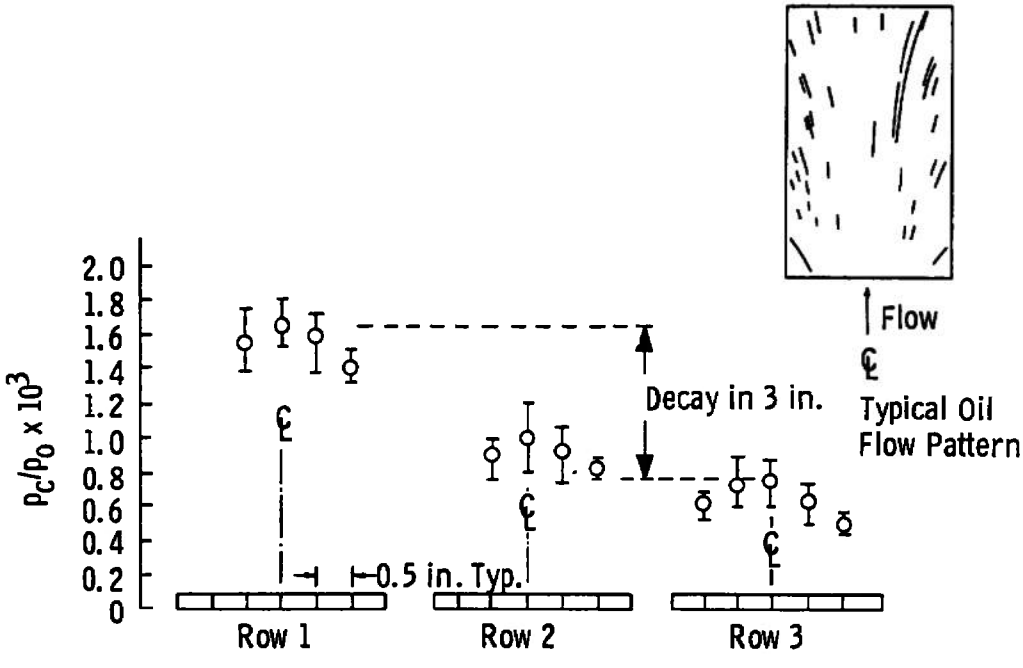

b. Across Model

Fig. 14 Combustor Section Pressure Distribution (Model without Sidewalls)

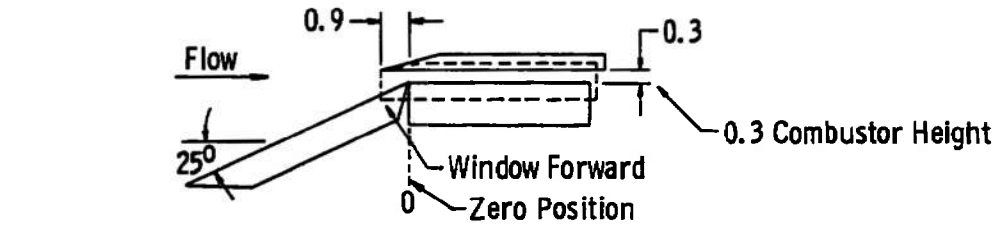

a. Configuration A

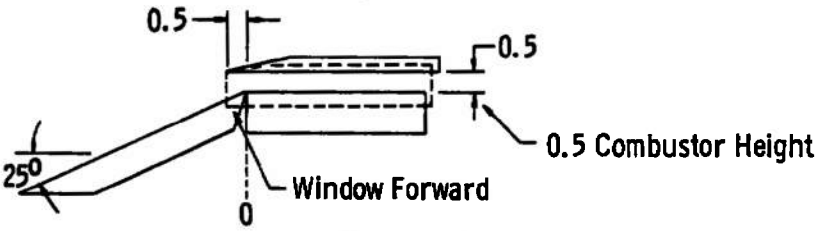

b. Configuration B

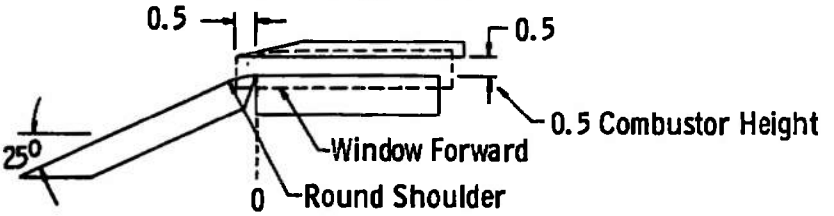

c. Configuration C

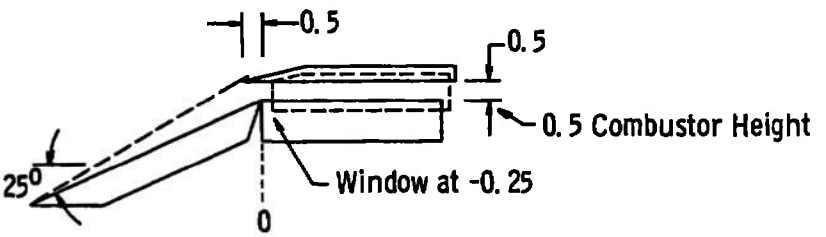

d. Configuration D

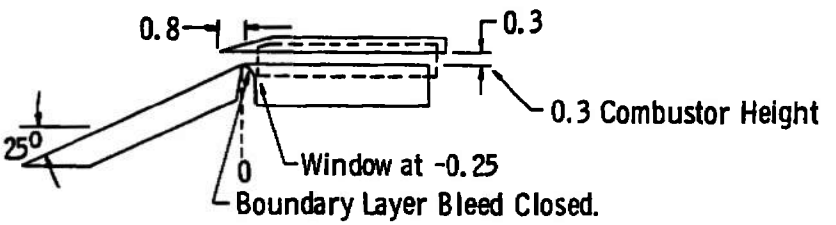

e. Configuration E

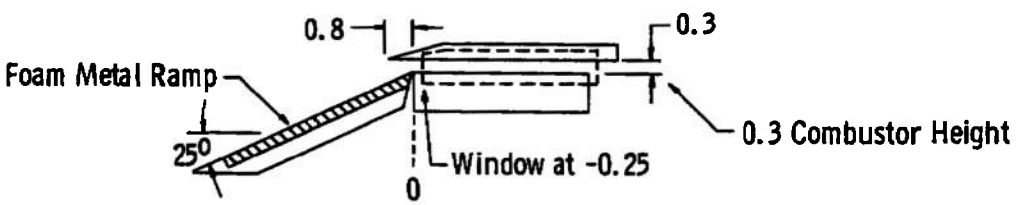

f. Configuration F

Fig. 15 Model Configurations (with Sidewalls)

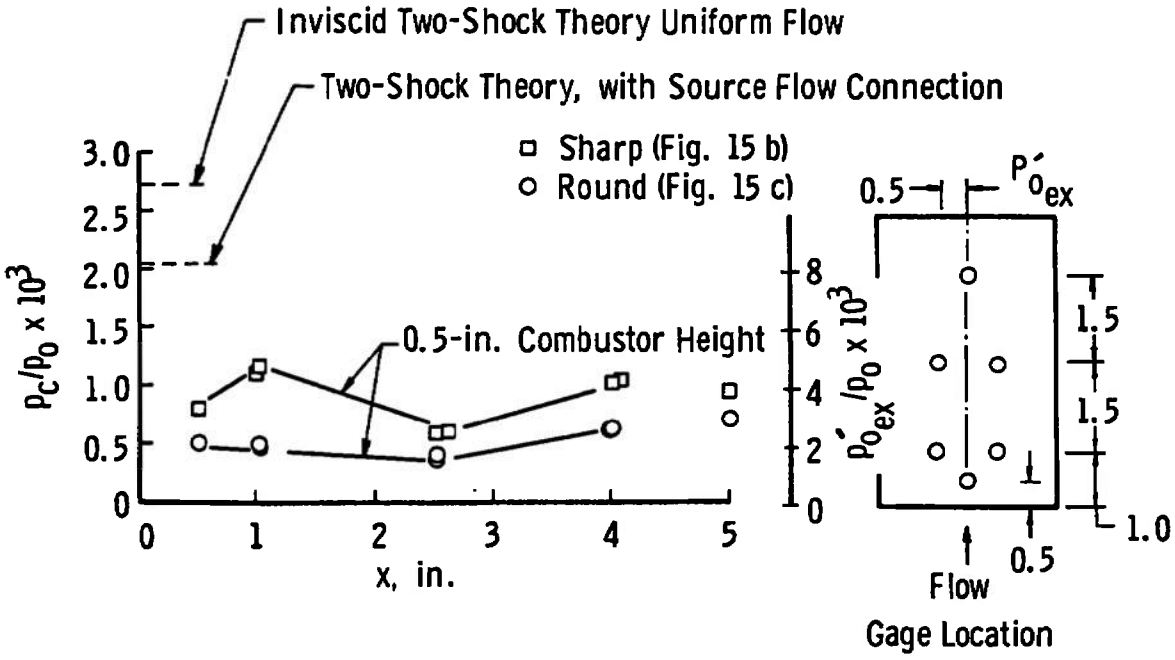

a. Effect of Shoulder Shape

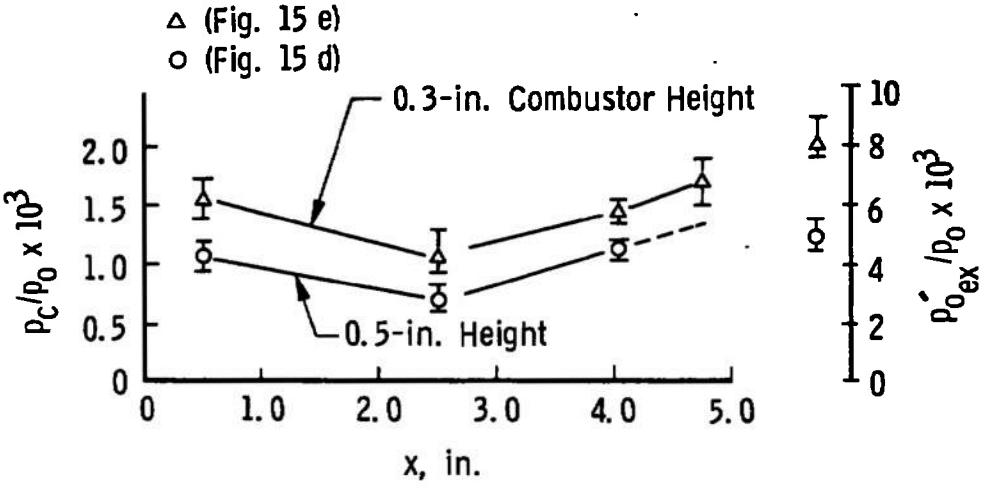

b. Effect of Combustor Height

Fig. 16 Effect of Shoulder Shape and Combustor Height on Combustor Pressure

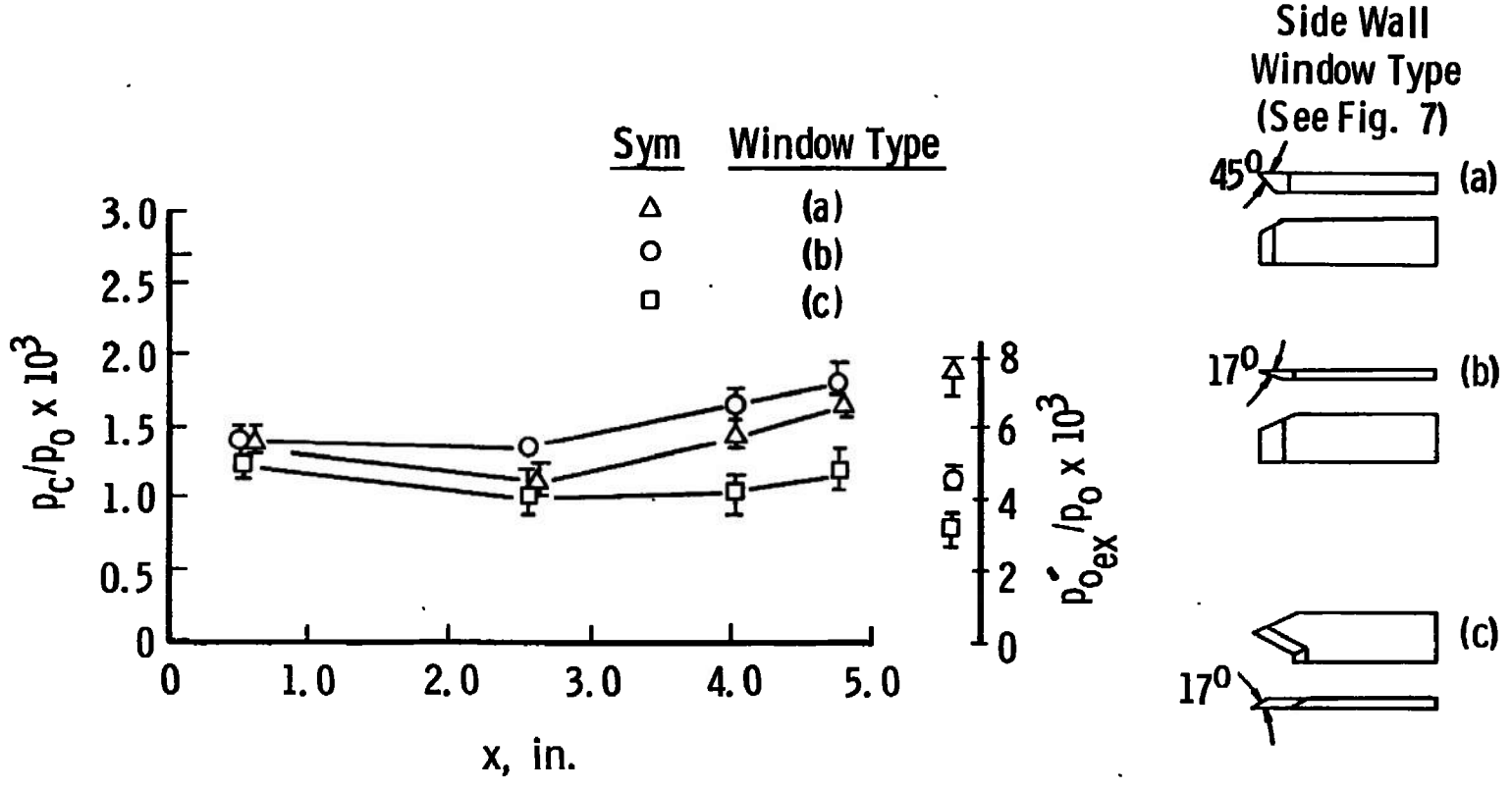

Fig. 17 Effect of Sidewall Leading-Edge Angle on Combustor Pressure

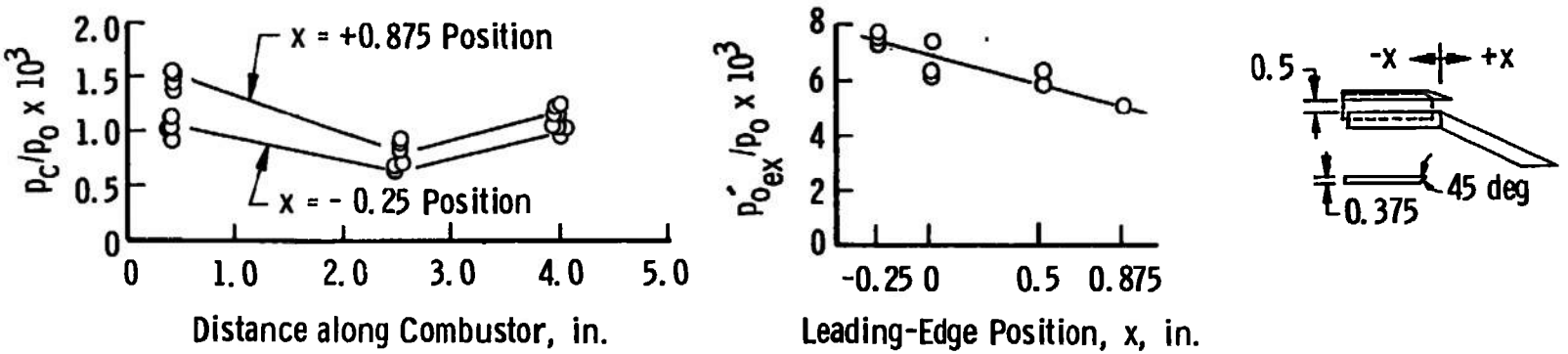

a. 45-deg Leading Edge

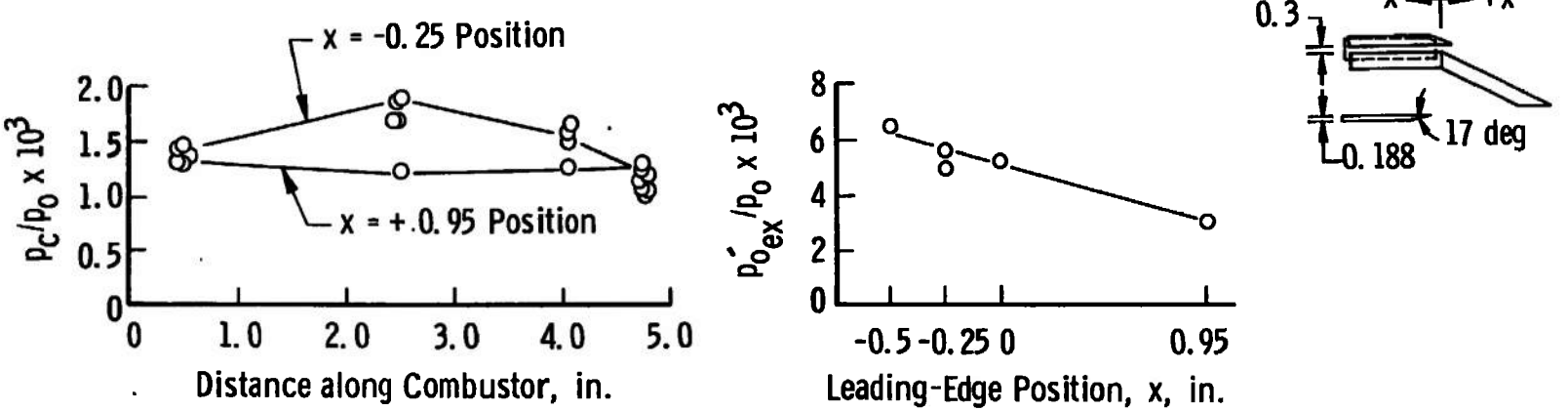

b. 17-deg Leading Edge (Steel)

Fig. 18 Effect of Sidewall Position on Combustor Pressure

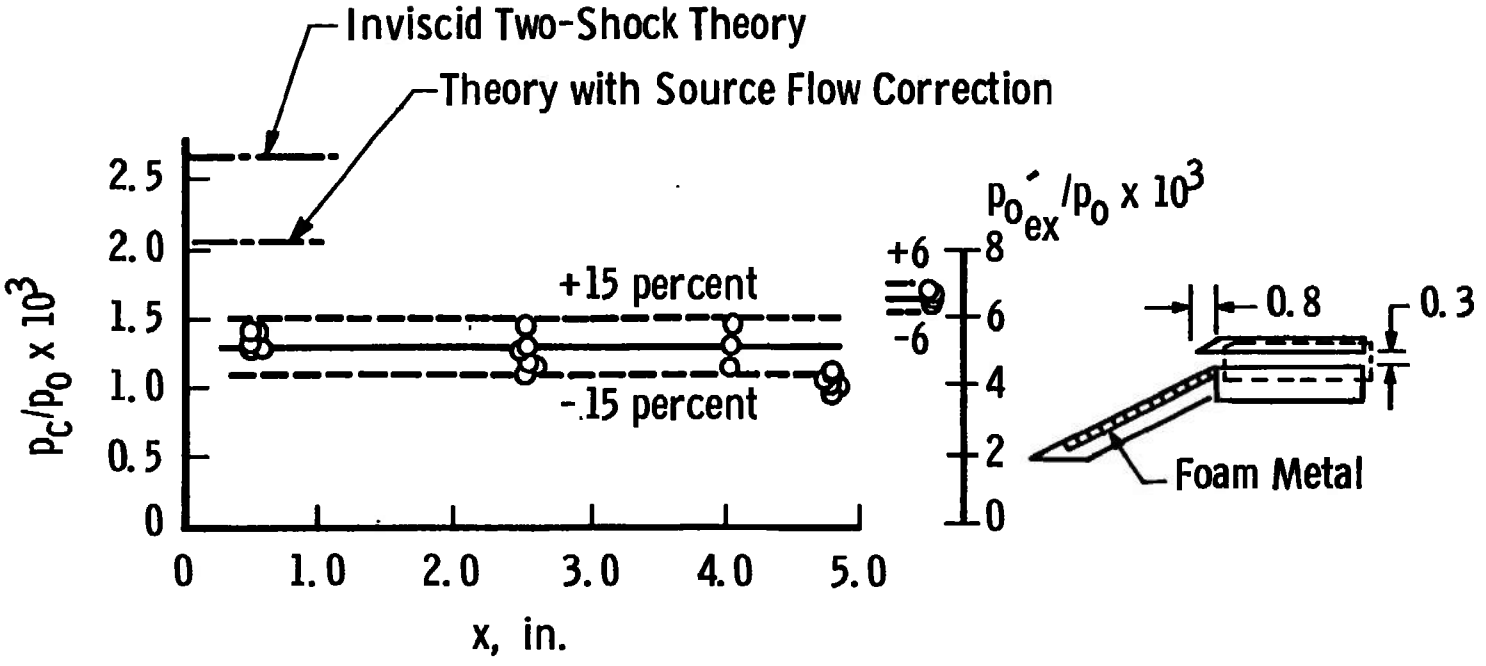

Fig. 19 Effect of Porous Inlet Ramp on Combustion Section Pressure

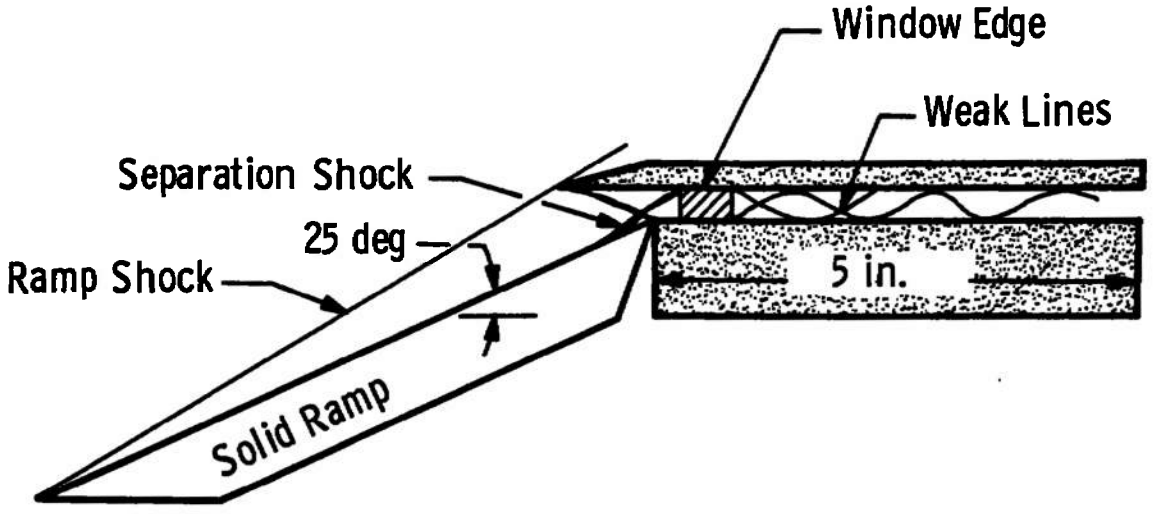

a. Solid Ramp

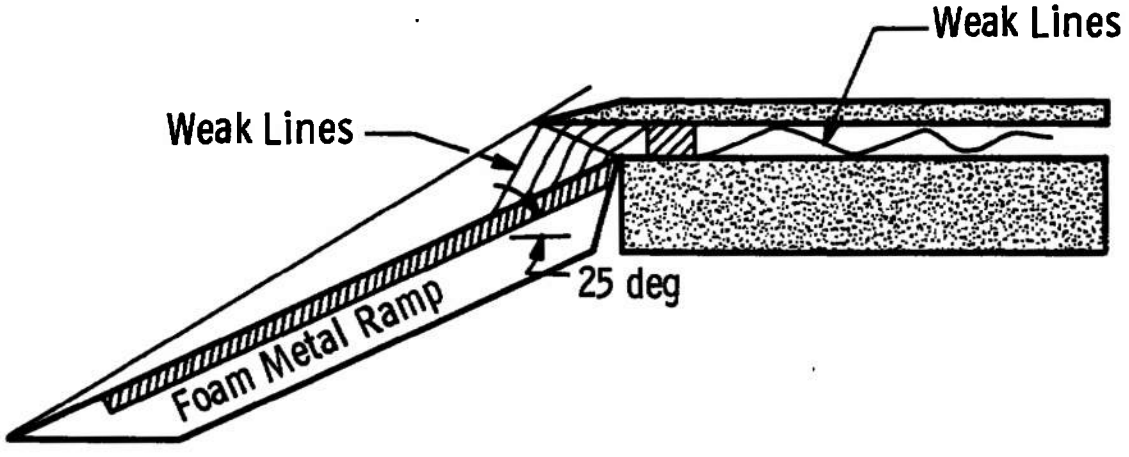

b. Foam Metal Ramp

Fig. 20 Comparison of Shock Patterns for Solid and Foam Metal Ramps

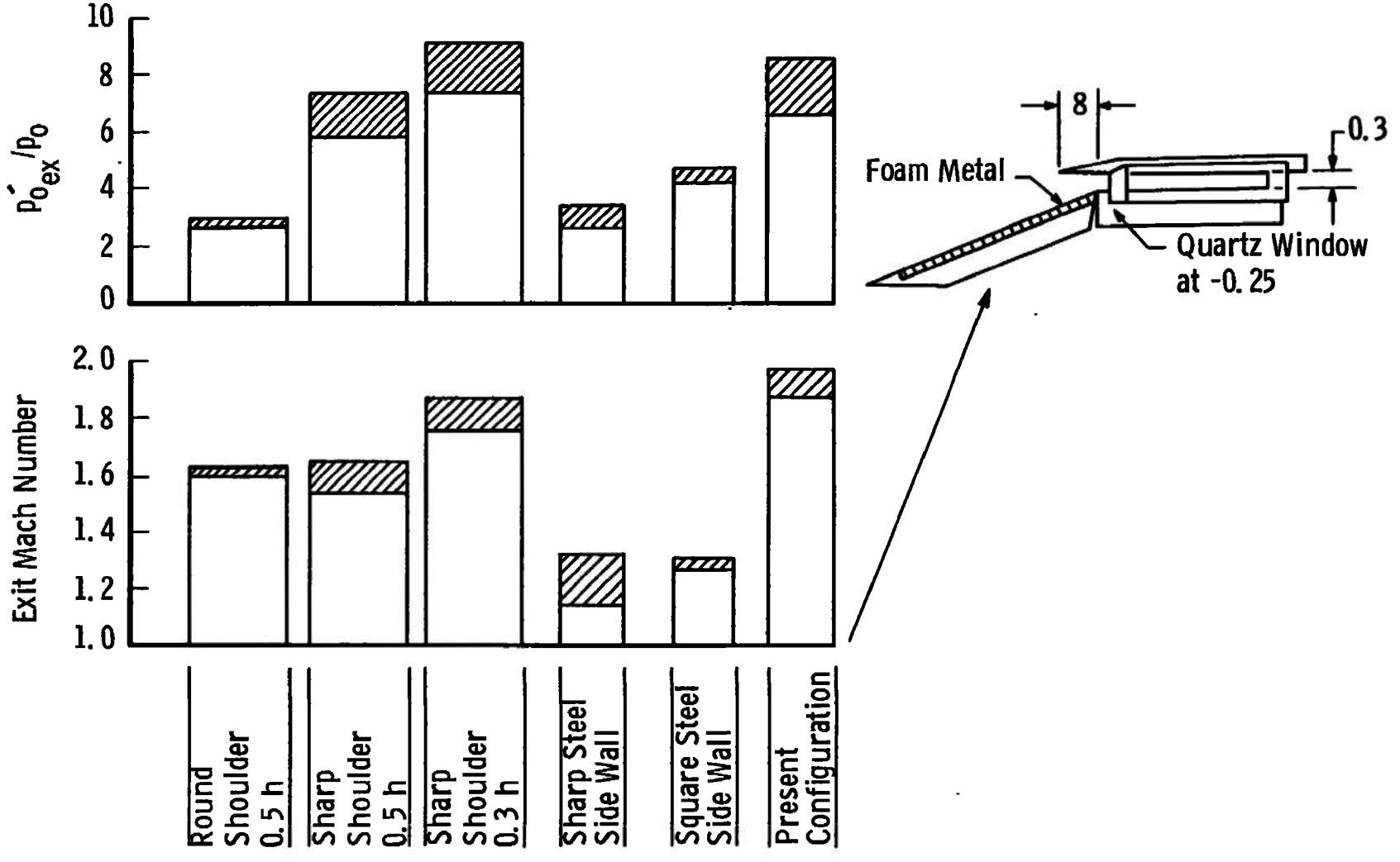

Fig. 21 Pitot Pressures and Mach Numbers for Various Configurations

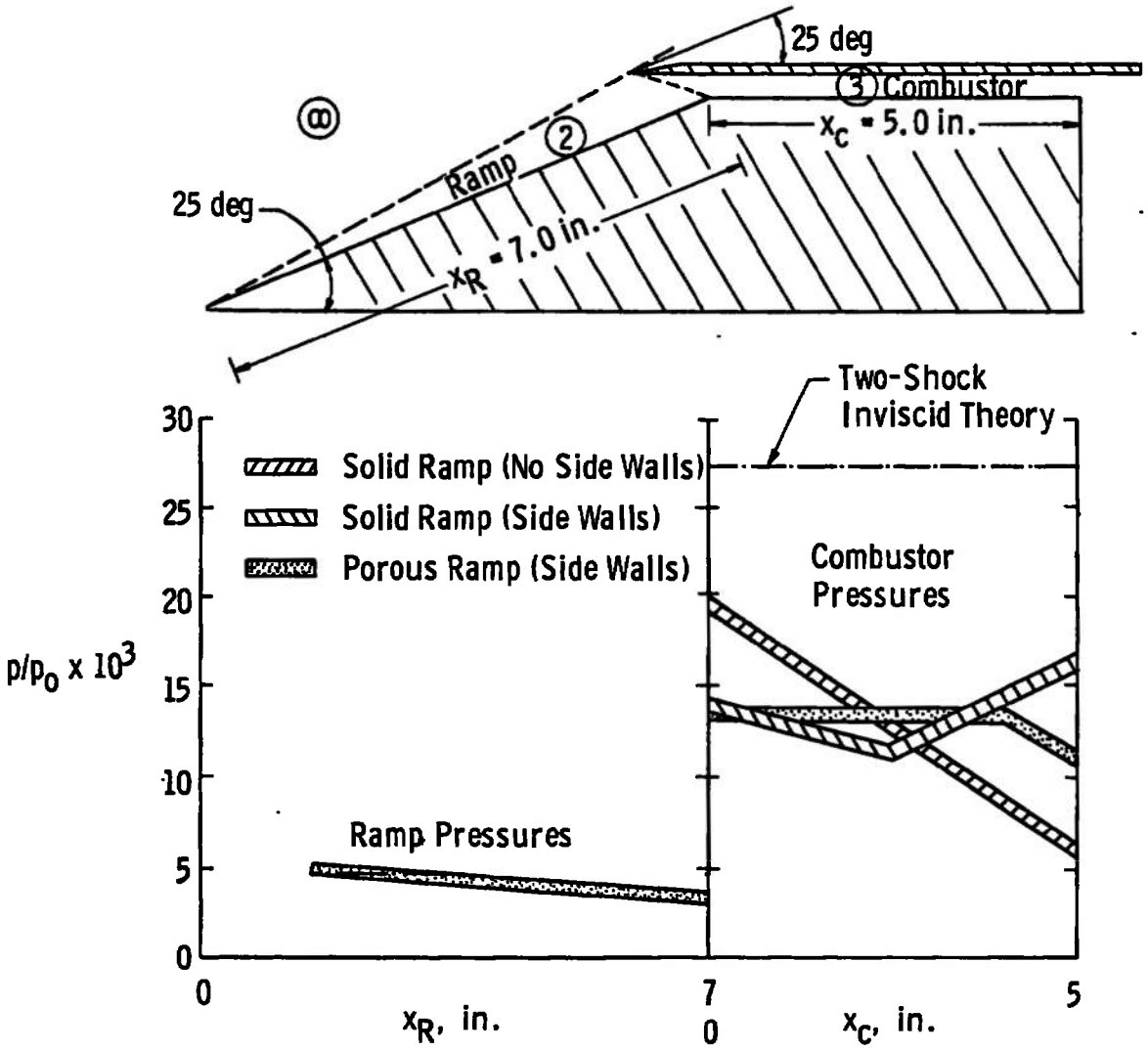

Fig. 22 Summary of Static Pressure in the Combustor

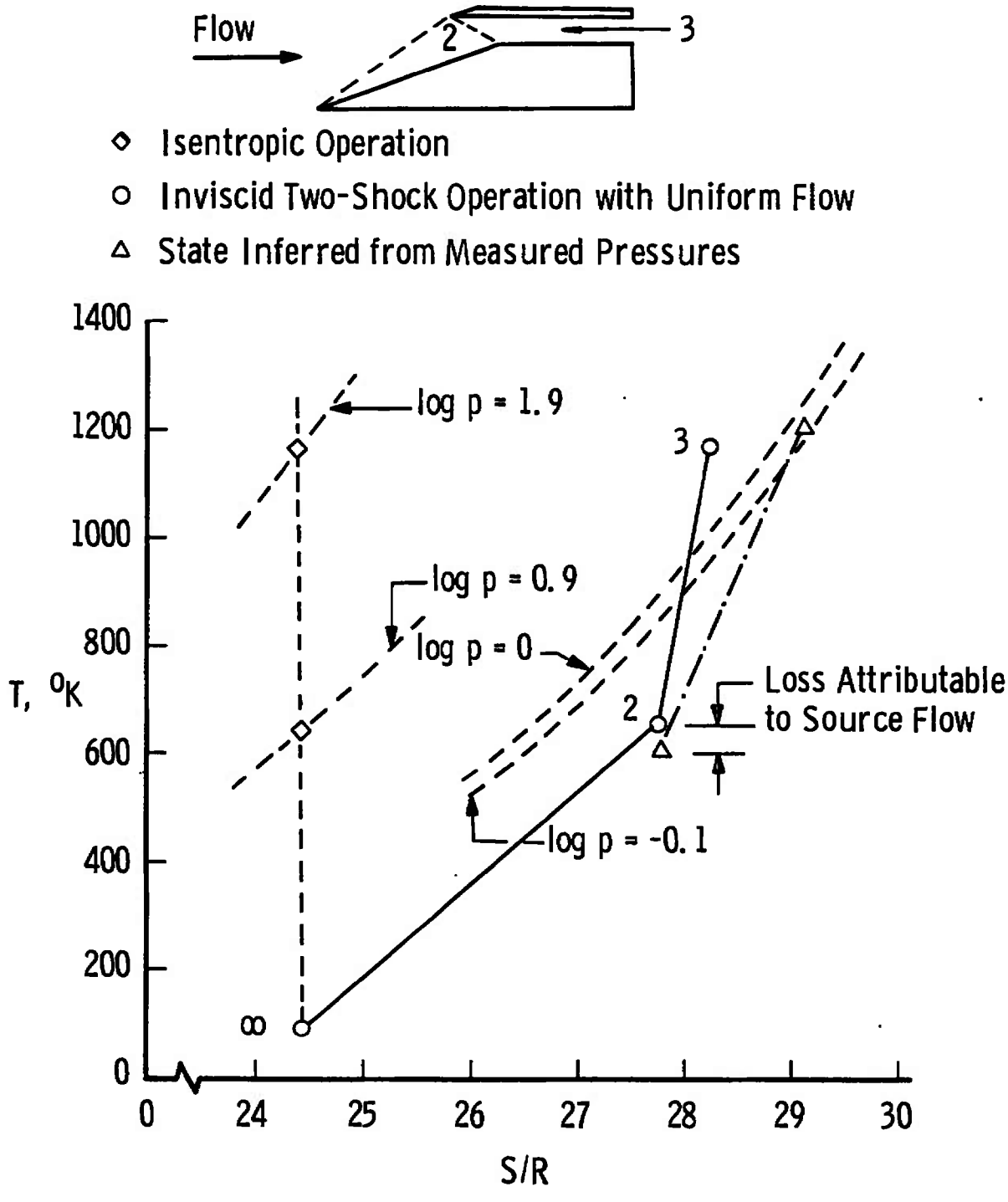

Fig. 23 Mollier Diagram for a Double-Oblique-Shock Inlet

TABLE I
TYPICAL RUN CONDITIONS

Initial Driver Pressure	13,000 psia
Initial Driven Tube Pressure	108 psia
Primary Shock Mach Number (M_S)	3.83
Reservoir Conditions	
Reflected Shock Pressure, p_{5s}	708 atm
Reflected Shock Temperature, T_{5s}	1860°K
Free-Stream Conditions	
Pressure, p_∞	0.00817 atm (0.12 psia)
Temperature, T_∞	88°K
Velocity, U_∞	6789 ft/sec
Reynolds Number, Re_∞/ft	3.38×10^6
Mach Number, M_∞	11

TABLE II
MODEL DESIGN CONDITIONS
TWO-SHOCK THEORY (INVISCID)

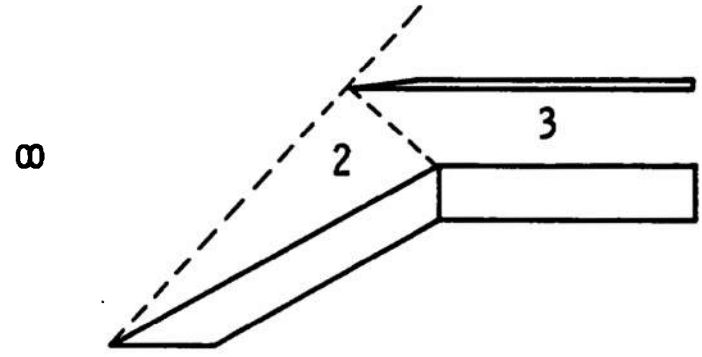

	∞	2	3
p (psia)	0.12	4.8	27.3
T (°K)	88	647	1160
M	11.0	3.5	2.1
U (ft/sec)	6789	5819	4635
τ_{id} (μsec)	---	---	17
τ_R (μsec)	---	---	10
L_o (in.)	---	---	1.50

τ_{id} = ignition delay for premixed hydrogen-air

τ_R = reaction time

L_o = length of combustor for complete reaction = $u_3 \times (\tau_{ID} = \tau_R)$

∞ = free stream

2 = conditions on inclined flat plate ramp

3 = conditions in combustor.

APPENDIX III
IGNITION DELAY AND REACTION TIME

Expressions which describe ignition delay and reaction time for combustion of hydrogen in air (premixed) have been given in Ref. 11. These expressions are, respectively

$$p\,\tau_{ID} = 0.008\, e^{9600/T} \qquad \text{(III-1)}$$

and

$$p^{1.7}\,\tau_R = 105\, e^{-1.12T/1000} \qquad \text{(III-2)}$$

where

p = static pressure, atm
T = static temperature, °K
τ_{ID} and τ_R = time, μsec

Both equations were established for a pressure range of from 0.2 to 5 atm and an initial temperature range of 1000 to 2000°K. The ranges of equivalence ratios, ER, are:

$$\text{Eq. (III-1)}\quad 0.4 \leq \text{ER} \leq 2.0$$

$$\text{Eq. (III-2)}\quad 0.3 \leq \text{ER} \leq 1.2$$

where

$$\text{ER} = \frac{\text{Fuel–Air Ratio}}{\text{Stoichiometric Fuel-Air Ratio}}$$

APPENDIX IV
LAMINAR HEAT-TRANSFER CORRELATION

HEAT-TRANSFER RATES - LAMINAR BOUNDARY LAYER

The local skin friction coefficient for a compressible laminar boundary layer is given by the equation

$$C_f = \frac{0.664}{\sqrt{Re_x}} \sqrt{\frac{\rho^* \mu^*}{\rho_2 \mu_2}} \qquad \text{(IV-1)}$$

which is a modification to the Blasius solution for incompressible flow over a flat plate. The asterisk denotes that the properties are to be evaluated at the Eckert reference enthalpy given by

$$h^* = 0.5\,(h_2 - H_w) + 0.22\,(h_r - h_2) \qquad \text{(IV-2)}$$

where h_r is the recovery enthalpy defined by:

$$h_r = h_2 + \sqrt{Pr^*}\, U_2^2/2 \qquad \text{(IV-3)}$$

By definition, the Stanton number is

$$C_{H_2} = \frac{\dot{q}_w \ell}{\rho_2 U_2 (h_r - H_w)} \qquad \text{(IV-4)}$$

and is assumed to be related to the skin friction coefficient by the modified Reynolds analogy:

$$C_{H_2} = (Pr^*)^{2/3} \cdot \frac{C_f}{2} \qquad \text{(IV-5)}$$

Substitution of Eq. (IV-1) into (IV-5) gives

$$C_{H_2} \sqrt{Re_x} = 0.332\, (Pr^*)^{-2/3}\, \frac{\rho^* \mu^*}{\rho_2 \mu_2} \qquad \text{(IV-6)}$$

Applicability of Eq. (2), p. 7, which was suggested by Whitfield,* results from the following assumptions;

1. Linear viscosity law; $\frac{\rho^* \mu^*}{\rho_2 \mu_2} = 1$
2. Prandtl number of unity, thus $H_o = h_r$
3. Hypersonic approximations are applicable; large Mach number, small deflection angles, and small changes in velocity

*J. D. Whitfield, ARO, Inc., Chief of the von Karman Gas Dynamics Facility, AEDC.

Thus

$$\frac{C_{H_2}}{C_{H_\infty}} = \frac{\dfrac{\dot{q}_{w\ell}}{\rho_2 U_2 (h_r - H_w)}}{\dfrac{\dot{q}_w}{\rho_\infty U_\infty (H_o - H_w)}} \approx \frac{\rho_\infty}{\rho_2} \qquad \text{(IV-7)}$$

The ratio of the ramp and free-stream Reynolds numbers is approximated as

$$\frac{Re_{2x}}{Re_{\infty_x}} \approx \frac{\rho_2 \mu_\infty}{\rho_\infty \mu_2} \approx \frac{\rho_2}{\rho_\infty} \frac{T_\infty}{T_2}$$

Therefore,

$$\frac{C_{H_2}}{C_{H_\infty}} \frac{\sqrt{Re_{2x}}}{\sqrt{Re_{\infty_x}}} = \sqrt{\frac{p_2}{p_\infty}} \qquad \text{(IV-8)}$$

Substituting Eq. (IV-6) into (IV-8) gives

$$C_{H_\infty} \sqrt{Re_{\infty_x}} \approx 0.332 \sqrt{p_2/p_\infty} \qquad \text{(IV-9)}$$

The local heat-transfer rate to the wall is then

$$\dot{q}_{w\ell} = 0.332 \rho_\infty U_\infty (H_o - H_w) \sqrt{Re_{\infty_x}} \sqrt{p_2/p_\infty} \qquad \text{(IV-10)}$$

UNCLASSIFIED

Security Classification

DOCUMENT CONTROL DATA - R & D

(Security classification of title, body of abstract and indexing annotation must be entered when the overall report is classified)

1. ORIGINATING ACTIVITY *(Corporate author)*
Arnold Engineering Development Center
ARO, Inc., Operating Contractor
Arnold Air Force Station, Tennessee 37389

2a. REPORT SECURITY CLASSIFICATION
UNCLASSIFIED

2b. GROUP
N/A

3. REPORT TITLE
DEVELOPMENT OF A DOUBLE-OBLIQUE-SHOCK SCRAMJET MODEL IN A SHOCK TUNNEL

4. DESCRIPTIVE NOTES *(Type of report and inclusive dates)*
February 1967 to September 1968 Final Report

5. AUTHOR(S) *(First name, middle initial, last name)*
I. T. Osgerby, H. K. Smithson, and D. A. Wagner, ARO, Inc.

6. REPORT DATE	7a. TOTAL NO. OF PAGES	7b. NO. OF REFS
August 1969	55	13

8a. CONTRACT OR GRANT NO.	9a. ORIGINATOR'S REPORT NUMBER(S)
F40600-69-C-0001	AEDC-TR-69-59
b. PROJECT NO. 3012	
c. Task 07	9b. OTHER REPORT NO(S) *(Any other numbers that may be assigned this report)*
d. Program Element 62402F	N/A

10. DISTRIBUTION STATEMENT
This document has been approved for public release and sale; its distribution is unlimited.

11. SUPPLEMENTARY NOTES	12. SPONSORING MILITARY ACTIVITY
Available in DDC.	Arnold Engineering Development Center, Air Force Systems Command, Arnold AFS, Tennessee 37389

13. ABSTRACT

A double-oblique-shock scramjet model has been developed using the AEDC-VKF 16-in. Shock Tunnel I at a free-stream Mach number of 11. The model was developed as a test bed for the development of instrumentation and hydrogen fuel injection techniques for supersonic combustion experiments to be conducted at the 54-in. test section in the AEDC-VKF Tunnel F. Difficulties were encountered, especially at the entrance to the combustor because of the combined action of separation and the interaction of the second shock from the cowl lip. Considerable effort was expended before these influences were reduced to the point that the flow in the combustor was satisfactory. The results of these development tests are reported here.

DD FORM 1 NOV 65 1473

UNCLASSIFIED

Security Classification

14. KEY WORDS	LINK A		LINK B		LINK C	
	ROLE	WT	ROLE	WT	ROLE	WT
scramjet						
ramjet						
supersonic combustion						
wind tunnel tests						
models, development of						
hypersonic flow						

AFSC
Arnold AFS Tenn